LITHOS 514–515 (2025) 108168

Contents lists available at ScienceDirect

LITHOS

journal homepage: www.elsevier.com/locate/lithos

Shear zone memory revealed by in-situ Rb-Sr and $^{40}Ar/^{39}Ar$ dating of Pyrenean and Alpine tectonic phases in the external Alps

L. Boschetti [a,b,*], C. Boullerne [b], Y. Rolland [c], S. Schwartz [b], G. Milesi [d], D. Bienveignant [b], E. Macret [e,f], D. Charpentier [f], P. Münch [e], J. Mercadier [d], A. Iemmolo [e], P. Lanari [g], M. Rossi [c], F. Mouthereau [a]

[a] Géosciences Environnement Toulouse, Université de Toulouse Paul Sabatier, CNRS, IRD, 14 av. Edouard Belin, 31400 Toulouse, France
[b] ISTerre, Université Grenoble Alpes, USMB, CNRS, IRD, UGE, 38000 Grenoble, France
[c] EDYTEM, Université Savoie Mont Blanc, CNRS, UMR 5204, Le Bourget du Lac, France
[d] GeoRessources, Université de Lorraine, CNRS, LabCom CREGU, Vandoeuvre-lès-Nancy, France
[e] Géosciences Montpellier, Université de Montpellier, Université des Antillnes, CNRS, IRD, UMR 5243, Campus triolet cc060, Place E. Bataillon, 34095 Montpellier, France
[f] Chrono-environnement, Université Bourgogne Franche-Comté, CNRS, UMR6249, 25000 Besancon, France
[g] Institute of Earth Sciences, University of Lausanne, Géopolis, Quartier Mouline, 1015 Lausanne, Switzerland

ARTICLE INFO

Keywords:
Ductile deformation
Multiple system dating
Alpine tectonics
Shear zone activity

ABSTRACT

The combination of Rb-Sr and $^{40}Ar/^{39}Ar$ dating methods with high-resolution mineralogical investigation allows deciphering the multiphase history of shear zones and serves as a tool for tectonic reconstructions. However, the interpretation of dates obtained by these two methods in relation to cooling, fluid circulation or to deformation-induced (re)crystallization remains controversial. Here, we apply the in situ $^{87}Rb/^{87}Sr$ and $^{40}Ar/^{39}Ar$ dating methods to shear zone minerals used together with step heating $^{40}Ar/^{39}Ar$ dating in several case studies with contrasting structural and metamorphic histories along the External Crystalline Massifs (ECMs) of the SW Alps. Our results emphasize polyphase deformation and highlight a variable behaviour of Rb-Sr and K-Ar systems in shear zones. This study provides new constraints about the timing, conditions and mechanisms of deformation in the southern ECMs of the Western Alps. The inherited crustal-scale Variscan shear zones have been reactivated several times in a thick-skin mode since the Late Cretaceous. An early N-S compressional phase impacted the SW Alps mainly at around ~80–70 and ~40 Ma in the Argentera and Pelvoux shear zones, but this signal is not documented further north. This signal is better preserved in the southern Pelvoux massif, with a Rb-Sr age of 79.7 ± 3.7 Ma. There is also a significant compressional deformation on the W-Alpine scale at 34–32 Ma, associated with underthrusting beneath the Penninic Frontal Thrust (PFT). Two compressional deformation pulses occur at 26 and 22–20 Ma in the southern Argentera Massif, corresponding to the onset of transpressive deformation induced by the anti-clockwise rotation of the Adriatic Plate. Finally, the last phase of deformation around 18–15 Ma concerns only the NW Alps, in the Beaufortain massif, which was buried under the Mont-Blanc massif, during the propagation of deformation leading to the development of the frontal fold and thrust belt of the SW Alps. Our results also show that the southern Pelvoux massif already reached a temperature around 300 °C at a depth of 10–15 km depth during the Late Cretaceous. This range of temperature and pressure conditions is broadly similar to that reached in the ECMs during the Cenozoic deformation stages.

* Corresponding author at: Géosciences Environnement Toulouse, Université de Toulouse Paul Sabatier, CNRS, IRD, 14 av. Edouard Belin, 31400 Toulouse, France.
E-mail addresses: louise.boschetti@univ-tlse3.fr (L. Boschetti), yann.rolland@univ-smb.fr (Y. Rolland), stephane.schwartz@univ-grenoble-alpes.fr (S. Schwartz), gaetan.milesi@univ-lorraine.fr (G. Milesi), dorian.bienveignant@univ-grenoble-alpes.fr (D. Bienveignant), eric.macret@univ-fcomte.fr (E. Macret), delphine.charpentier@univ-fcomte.fr (D. Charpentier), philippe.munch@umontpellier.fr (P. Münch), Julien.mercadier@univ-lorraine.fr (J. Mercadier), arthur.iemmolo@umontpellier.fr (A. Iemmolo), pierre.lanari@unil.ch (P. Lanari), magalie.rossi@univ-smb.fr (M. Rossi), frederic.mouthereau@get.omp.eu (F. Mouthereau).

https://doi.org/10.1016/j.lithos.2025.108168
Received 20 February 2025; Received in revised form 20 June 2025; Accepted 24 June 2025
Available online 28 June 2025

1. Introduction

Shear zones potentially preserve the memory of multiple deformation and hydrothermal events and may be used as tracers of tectonic and thermal evolution of orogens (e.g. Monié et al., 2023). These high strain zones allow deciphering different deformation stages in upper to middle crust at the brittle-ductile transition by the study of *syn*-kinematic mica and chlorite (Di Vincenzo et al., 2004). Fluid-rock reaction largely results in the neocrystallization of mica and chlorite at the expanse of feldspars (e.g., Rolland et al., 2008). To trace the history of shear zones activity, it becomes possible to combine several analytical methods: (i) in situ $^{40}Ar/^{39}Ar$ and Rb-Sr dating of white mica, in which a short wavelength laser is used to ablate small (~100 μm^3 size) and spatially controlled volumes of material, and the step heating $^{40}Ar/^{39}Ar$ method allowing to evaluate the homogeneity of the Ar signal and the temperature-age relationships (e.g., Kellett et al., 2024; Sanchez et al., 2011a) and (ii) chemical maps of mineral assemblages using Electron Probe Micro Analysis (EPMA) allowing a spatial estimate of Pressure and Temperature at a 10 µm scale (Lanari et al., 2012, 2013, 2014). This multi-method approach is valuable to dating deformation and/or fluid circulation in addition to a detailed chemical analysis of structural domains, which results in the mapping of intra-grain age and Pressure-Temperature (P-T) distributions (e.g., Kellett et al., 2016; Schneider et al., 2013). Up to now, still few studies (e.g., Kellett et al., 2024) have applied this multi-method approach in the same samples, leaving questions about the consistency of the results and their specific relationship to deformation and fluid flow events.

The western alpine External Crystalline Massifs (ECMs) are a good example of a continental crust exhibiting several deformation phases. First-order structural inheritance in the Alps is emphasized by its high-grade subvertical anisotropy inherited from the SE Variscan shear zone network, imaged by recent deep geophysical surveys (Nouibat et al., 2022; Schwartz et al., 2024). This anisotropy has been reactivated several times during early Mesozoic rifting stages (Mohn et al., 2014),

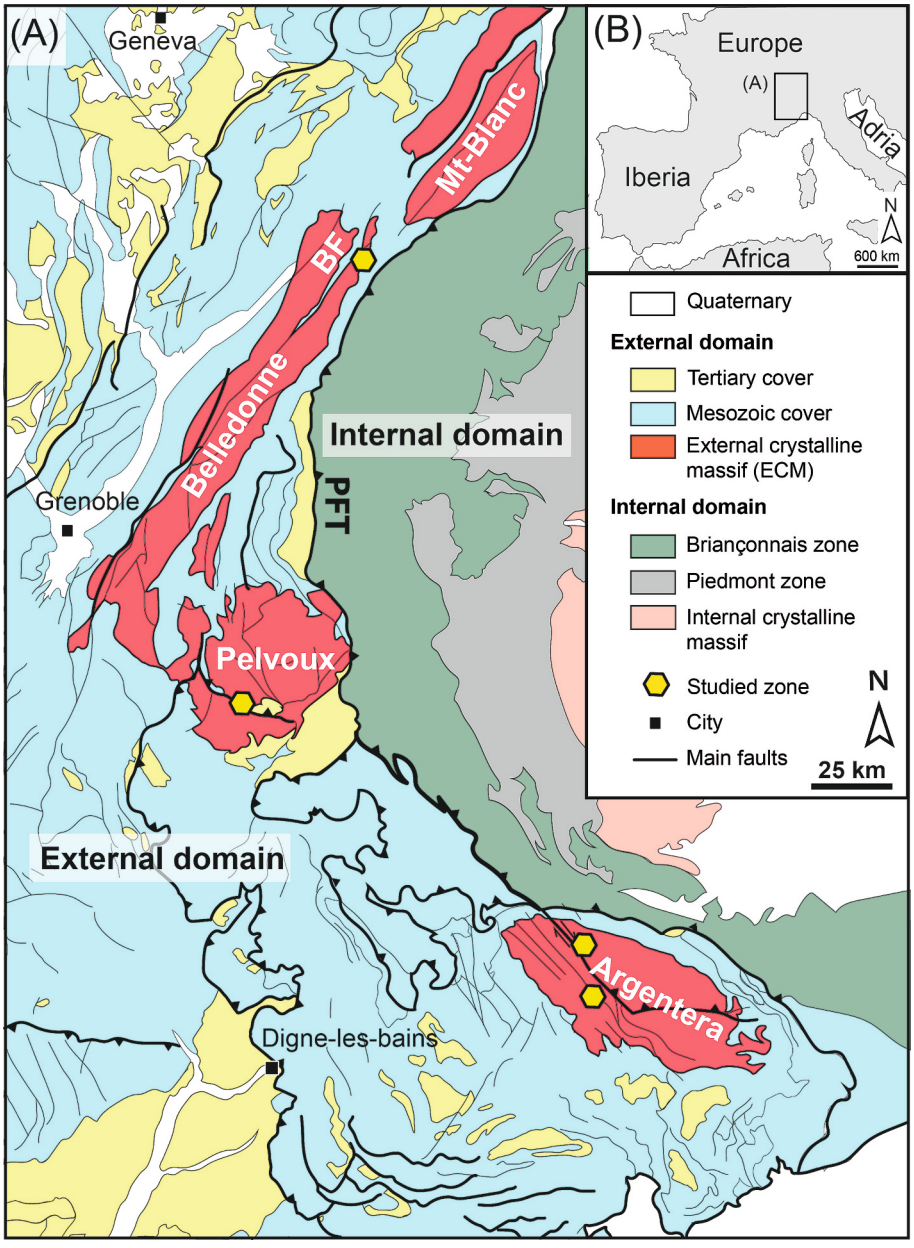

Fig. 1. A) Geological map of the Western Alps showing location of the External Crystalline Massifs, and of the studied shear zones. BF: Beaufortain Massif. B) general map of the Western Alps. PFT: Penninic Frontal Thrust.

and further during Late Mesozoic to Cenozoic 'Pyrenean' or 'Eo-alpine' (Bienveignant et al., 2024; Boschetti et al., 2025a; Montemagni et al., 2023) and Alpine (Bellahsen et al., 2014; Rolland et al., 2008, 2022; Simon-Labric et al., 2009) orogenic phases. This paper provides constraints on the polyphase tectonic activity and geothermal evolution of the Alpine orogen by investigating crustal-scale shear zones. These structures are used as geological markers of the successive tectonic phases. Syn-kinematic minerals, formed during shear zone activity, mainly chlorite and phengite, are studied coupling petrological and geochronological approaches to retrieve the P-T conditions and time frame of the deformation phases. For this, EPMA is used for chemical characterization associated with quantification, leading to mineralogical mapping and P-T estimates of deformation stages. In situ and step heating $^{40}Ar/^{39}Ar$ dating were applied together with in situ Rb-Sr geochronology, performed to determine the timing of deformation and/or fluid circulation events.

2. Geological setting

2.1. Context of shear zone deformation and Alpine evolution

The southwestern (SW) Alps (Fig. 1) result from the collision between the Adria and European plates, beginning during the upper Eocene (e.g., Agard and Handy, 2021 and references therein). From east to west, a progressive metamorphic gradient is observed. The external zone is emphasized with a weak metamorphism culminating in the greenschist up to lower amphibolite facies conditions (<400 °C, $P < 5$ kbar up to 550 °C 8–10 kbar), while the internal zone shows HP-LT metamorphism developed in a blueschist ($300 < T < 600$ °C, $5 < P < 12$ kbar) to eclogite facies conditions ($T > 550$ °C, $P > 12$ kbar) metamorphism (e.g., Ceccato et al., 2024; Nibourel et al., 2021 and references therein). The major structure of the SW Alps is the Penninic Frontal Thrust (PFT), a thrust that separates the internal units on its hanging wall from the external units further west on its footwall (e.g., Dumont et al., 2022; Rosenberg et al., 2021). The internal units (Fig. 1) were buried during the subduction of the European slab underneath the Adria plate and were subsequently exhumed during the Alpine collision by westward transport along the PFT. The external units, which extend all along the curvature of the Alpine arc, include the crystalline continental crust corresponding to the ECMs, and the overlying Mesozoic to Cenozoic sedimentary cover, partly decoupled from the basement and deformed along a frontal fold and thrust system (e.g., Bilau et al., 2023a; Schwartz et al., 2017). The ECMs of SW Alps, which occur as tectonic windows below the Mesozoic sedimentary cover, are mainly composed of exhumed Variscan basement. It is well known that the ECMs are cross-cut by major shear zones representing zones of mechanical weakness. These shear zones initially formed in the Variscan orogen, along the East Variscan Shear Zone network, a network of anastomosed N-S to NW-SE trending shear zone (e.g., Corsini and Rolland, 2009; Simonetti et al., 2018). This anisotropy has been reactivated during the alpine collision by localizing the deformation and facilitating the exhumation of ECMs (Tricart, 2004; Sanchez et al., 2011b; Lanari et al., 2012; Schwartz et al., 2024). Several works have well constrained the different steps of the Alpine deformation, mainly related to the activation of the Penninic Frontal Thrust (PFT) at ~34 Ma by underthrusting of continental crust until 27 Ma in the Aar, Gotthard, Mont blanc and Pelvoux ECMs (e.g., Bellanger et al., 2015; Ceccato et al., 2024; Cenki-Tok et al., 2014; Simon-Labric et al., 2009). However, some earlier deformation phases related to the Pyrenean-Provence orogeny have also affected the European crust, as evidenced by the foreland structuration affecting the sedimentary cover observed in the southern part of the SW Alps (Balansa et al., 2022; Boschetti et al., 2025a, In Press). Such deformation is exhibited by the Lure-Ventoux northward thrusting, and by globally northward fold succession in the Dévoluy and Baronnies massifs (Bienveignant et al., 2024). This pre-structuring of the European foreland has been associated with several Pyrenean-Provence (or Eo-Alpine) compressive phases from the Late Cretaceous to the Eocene (e.g., Balansa et al., 2022; Bilau et al., 2023b; Boschetti et al., 2025b; Parizot et al., 2022) and was largely overprinted by a higher metamorphic grade deformation in most of the ECMs. Some stratigraphic and structural insights demonstrate that the basement was also involved in this Cretaceous structuring in a thick-skin tectonic style (Bellahsen et al., 2014). In the Pelvoux ECM, two main compressive deformation phases are identified: (i) a first pre-Nummulitic (>37 Ma) north-south shortening (Boschetti et al., 2025a; Sue et al., 1997), followed by a second (ii) east-west shortening dated at 35–30 Ma (Bellanger et al., 2015; Simon-Labric et al., 2009), which is referred to as the 'Alpine' phase. The first north-south phase is identified in the basement, as it is uncomformably covered by the Priabonian 'Nummulitic Flysch' (Tricart, 2004; Fig. 2B, E). As a result of this early phase, the Mesozoic deposits of the southern Pelvoux massif are locally eroded and deformed prior to the Nummulitic transgression, which therefore suggests an uplift in the Late Cretaceous to Early Cenozoic. In the Dévoluy, north-south compressive structures highlighted by east-west folds and thrusts are cross-cut by a Senonian unconformity, in agreement with a Late Cretaceous age for the Pyrenean compression (e.g., Ford et al., 2022). Thermal histories reconstructed in the southern Pelvoux and the NW part of the Argentera ECMs indicate an early Pyrenean-Provence phase in the Late Cretaceous-Paleogene consistent with Zircon Fission Tracks (ZFT) cooling ages in the range ~85–40 Ma (Bigot-Cormier et al., 2006; Boschetti et al., 2025a). Despite the detailed characterization of the Alpine (stricto sensu) and Pyrenean-Provence events, uncertainties remain regarding the polyphase crustal thickening of the ECMs and the associated P-T conditions. In addition, the reactivation of ductile shear zones has yet to be fully characterized due to a lack of constraints. The 'Alpine' (stricto sensu) deformation has been widely described in previous works, but the impact and extent of the Pyrenean-Provence phase seems to be underestimated due to a lack of age constraints.

2.2. Investigated ECM shear zones

2.2.1. The Argentera ECM

The Argentera massif is the southernmost ECM of the SW Alps (Fig. 1). The massif is cross-cut by NW-SE oriented shear zones, the crustal-scale Bersezio (BSZ), Valetta-Mollières (VSZ) and Isola (ISZ) shear zones (Fig. 2A). These shear zones consist of a right-lateral system associated with subvertical NW-SE foliation inherited from the Variscan orogeny, which resulted in a dense network of subvertical NW-SE foliations (Fig. 2A). The ISZ and BSZ form a major dextral shear zone network separating two domains with distinct thermochronological histories. This network was reactivated multiple times during the Alpine orogeny. Low-temperature ductile reactivation occurred at 26, 22 and 20 Ma, in brittle-ductile to low-grade ductile conditions (Sanchez et al., 2011a), while after 20 Ma the brittle conditions took place (Sanchez et al., 2011b). Today, the BSZ is still tectonically active (e.g., Bauve et al., 2014; Sanchez et al., 2010). Pressure-temperature (P-T) estimations reached by the massif during deformation were obtained by using mineral multi-equilibria at 375 ± 30 °C and 4.8–7 ± 1 kbar (Sanchez et al., 2011a). These estimates correspond to the underthrusting of the massif below the PFT around ~34 Ma ($^{40}Ar/^{39}Ar$ dating on *syn*-kinematic phengites by Sanchez et al., 2011a). The subsequent massif's exhumation started around ~26–20 Ma (ZFT ages by Bigot-Cormier et al., 2006; $^{40}Ar/^{39}Ar$ dating on syn-kinematic phengites by Sanchez et al., 2011a). The putative main exhumation mechanism invoked in several studies (Bigot-Cormier et al., 2006; Sanchez et al., 2011b; Tricart, 2004) is a differential movement of rigid blocks within the Argentera (Fig. 2A), along the shear zones of the massif, coupled with an increasing uplift towards the NE, under a dextral-transpressive regime (Sanchez et al., 2011b). In the western part of the massif, the ZFT ages were not reset during underthrusting and show some ages in the range of ~84–50 Ma, suggesting an older exhumation event (Bigot-Cormier et al., 2006, Fig. 2A).

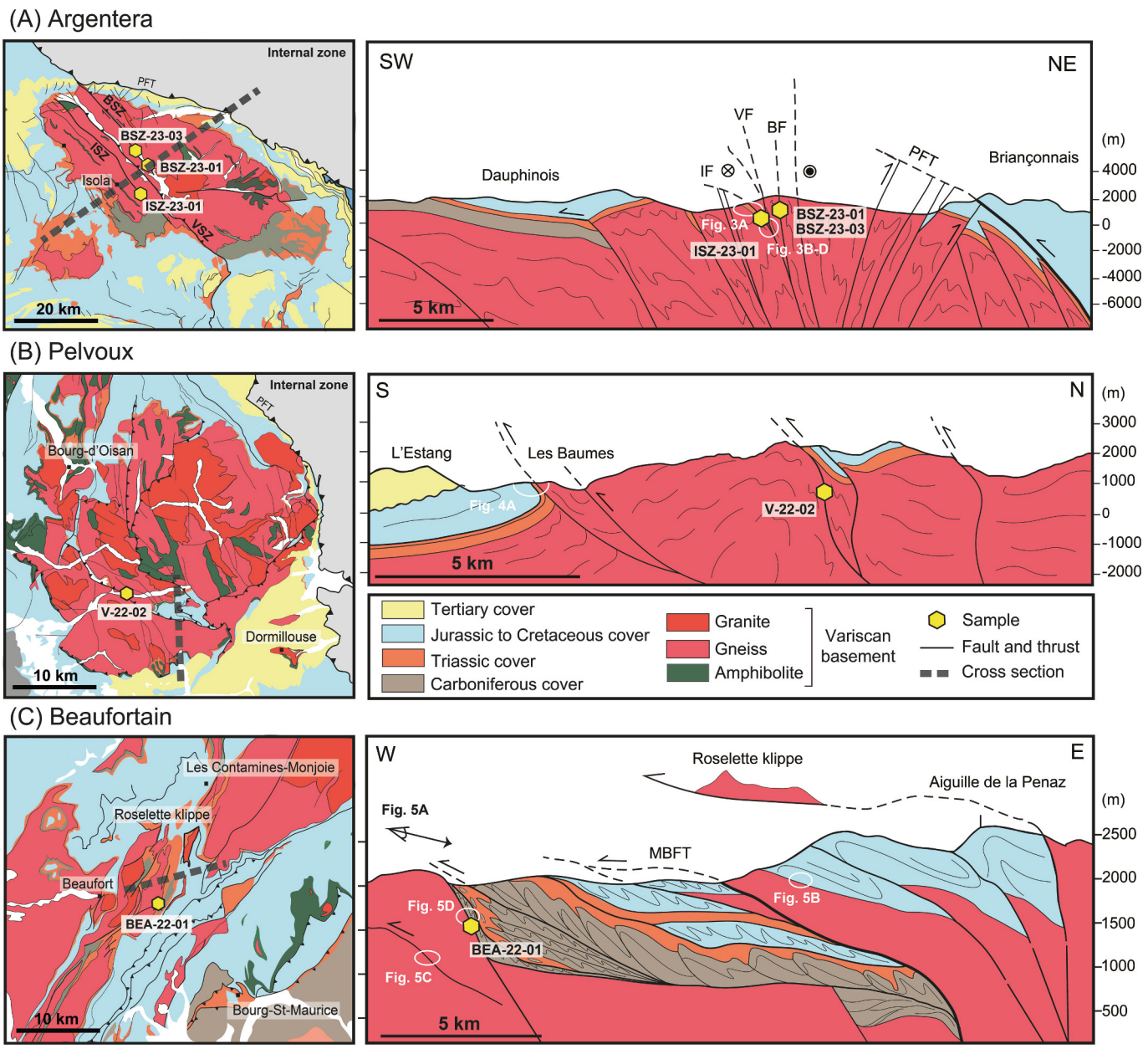

Fig. 2. Geological maps of investigated sites in this study. A) Geological map of the Argentera Externnal Crystalline Massif (ECM) and its corresponding geological cross section. B) Geological map of the Pelvoux ECM its corresponding geological cross section. C) Geological map of the Beaufortain ECM its corresponding geological cross section. Shear zones: Isola (ISZ); Valetta (VSZ); Bersezio (BSZ). PFT: Penninic Frontal Thrust. Locations of investigated sites are indicated on Fig. 1.

2.2.2. *Pelvoux ECM*

In the Pelvoux massif (Fig. 1, Fig. 2B), the tectonic inheritance from the Variscan orogeny is highlighted by north-south strike-slip faults corresponding to the East Variscan Shear Zone network (e.g., Corsini and Rolland, 2009; Simonetti et al., 2018). These faults were reactivated during the Jurassic rifting phase and were later inverted during the Alpine east-west compression. The Pelvoux ECM is also structured by inherited top-to-north or south thrusts (Fig. 2B) related to the Pyrenean-Provence compression that are not observed in the other ECMs (Lazarre, 1997; Tricart, 2004, Dumont et al., 2022). The earlier (Late Cretaceous) phase of exhumation is marked by an erosion surface on the basement and the entire Mesozoic cover is missing (Tricart, 2004). Within the Pelvoux massif, the estimated peak metamorphic P-T conditions are in the range of ~270–350 °C, corresponding to a depth of ~10–15 km (Bellahsen et al., 2014). A thermal inheritance difference between the south and north Pelvoux ECM is noted based on ZFT and apatite fission tracks (AFT) cooling ages. In the northeastern part, a reset of ZFT ages occurs, while the southern part still records an exhumation period between ~85–40 Ma below 350 °C to surface conditions (Boschetti et al., 2025a). This stage of exhumation is interpreted as the result of north-south Pyrenean-Provence compression.

2.2.3. *Beaufortain ECM*

In the Beaufortain massif (Fig. 2C), the tectonic inheritance from the Variscan orogeny is highlighted by north-south trending subvertical foliation and faults. These faults host some thick Carboniferous basins and were reactivated as normal faults during the Tethyan Jurassic rifting phase (Dall'Asta et al., 2022; Ribes et al., 2020). For this reason, the geometry of the crystalline basement exhibits an offset caused by Jurassic normal faulting, which was later subsequently overprinted during the Alpine compressional deformation. Further, the thickness of Mesozoic sediments is variable, resulting in the effect of *syn*-depositional

sediments during the Jurassic rifting phase. The tectonic inversion of this rift structure resulted in an intense vertical flattening, as evidenced by a steep cleavage along the previous north-south faults and the development of top-to-west shear zones, which cross-cut the basement or localize at the basement-cover interface (Fig. 2C).

3. Methods

3.1. Sampling strategy

From south to north, shear zones in the Argentera, Pelvoux, and Beaufortain massifs were studied to investigate the evolution and activity of shear zones along the western Alpine arc. In the Argentera massif, two samples were collected from the BSZ and one from the ISZ (Fig. 2A). Additionally, one sample was taken from the Valgaudemar shear zone in the Pelvoux massif (Fig. 2B) and one from a shear zone parallel to the Alpine prism and the Mont Blanc frontal thrust in the Beaufortain massif (Fig. 2C). Samples were then prepared as 100 μm thick sections and their mineralogy was characterized under a microscope from ISTerre Grenoble laboratory to complete the field structural investigation and to prepare dating.

3.2. Mineral chemistry and themobarometry

Chemical analyses were performed using the Electron Probe Micro-Analyzer (EPMA) JXA-iHP200F from the IMAP platform at the ISTerre Grenoble laboratory. Quantitative point analyses were made at 15 keV and 10 nA. Conditions for X-ray were fixed at 15 keV, 100 nA, dwell time of 200 ms, for a surface area of about 300 × 300 μm with a step of 0.5 μm. Raw X-ray maps were converted into oxide wt% maps using point analyses measured on the map area as internal standards with the software XMapTools 3.4.1 (Lanari et al., 2014). Structural formulae were then calculated for each pixel on a 14-oxygen basis and 11-oxygen basis for chlorite and phengite, respectively. Since Mg and Fe contents in chlorite are temperature dependent and Si and Na contents in phengite are pressure and temperature dependent (Lanari et al., 2012), structural formulae maps expressed in atoms per formula unit (apfu) elements were used to guide the thermobarometric investigations. The pressure-temperature (P-T) conditions of mineral formations were estimated using the Chl + Qz + H_2O calibration of Vidal et al. (2005) for chlorite and the Phg + Qz + H_2O calibration of Dubacq et al. (2010) for phengite (mineral abbreviations are according to Warr (2021), except for phengite, which is Phg). Following Lanari et al. (2012), the P-T conditions of the assemblage were determined by the intersection of the two methods in the P-T space. The thermodynamic calculations were performed with the program ChlMicaEqui (Petroccia et al., 2025).

3.3. $^{40}Ar/^{39}Ar$ dating

Two analytical techniques have been used in this work:

Step-heating $^{40}Ar/^{39}Ar$ technique was performed on phengite aggregates selected under a binocular microscope (size 500 μm). The grains were leached with HNO_3 (1 N) for a few minutes and then repeatedly cleaned ultrasonically in distilled water and alcohol. Samples were packed in aluminium foil for irradiation in the core of the Triga Mark II nuclear reactor of Pavia (Italy) with several aliquots of the Taylor Creek sanidine standard as flux monitor. Argon isotopic interferences on K and Ca were determined by irradiation of KF and CaF_2 pure salts from which the following correction factors were obtained: $(^{40}Ar/^{39}Ar)_K = 0.00969 \pm 0.00038$, $(^{38}Ar/^{39}Ar)_K = 0.01297 \pm 0.00045$, $(^{39}Ar/^{37}Ar)_{Ca} = 0.0007474 \pm 0.000021$ and $(^{36}Ar/^{37}Ar)_{Ca} = 0.000288 \pm 0.000016$. $^{40}Ar/^{39}Ar$ step-heating analyses were performed at Géosciences Montpellier (France). The gas extraction and purification line consist of (a) an IR-CO_2 laser of 100 kHz used at 3–20 % power to heat samples during 60 s, (b) a lens system for beam focusing, (c) a steel chamber maintained at 10–8 to 10–9 bar, with a copper holder in which 2 mm-diameter blind holes were milled, and (d) two Zr-Al getters for purification of gases. Argon isotopes are analyzed with an Argus VI multi-collection mass spectrometer (with 4 faraday cups for masses ^{40}Ar-^{37}Ar and one ion counting for ^{36}Ar). One minute was allowed for equilibration before analysis. Mass discrimination was monitored daily using an automated air pipette and ranged between 0.995012 and 0.999999 per Dalton (±0.0.03 %). Blank analyses were performed every three sample analyses. Raw data of each step and blank were processed and ages were calculated using the ArArCALC-software (Koppers, 2002). Isotopic ratios were corrected for irradiation interferences and air contamination using a mean air value $(^{40}Ar/^{36}Ar)_{atm}$ of 298.56 ± 0.31 (Lee et al., 2006; Renne et al., 2009). Ages are statistically analyzed in two ways: ^{39}Ar released spectra and inverse isochrones. Plateau ages are calculated from at least three consecutive ^{39}Ar release steps comprising up to 50 % of total $^{39}Ar_K$ released and overlapping at the 2σ confidence level. Inverse isochron ages are accepted when mean square weighted deviation (MSWD) is close to 1 and the $^{40}Ar/^{36}Ar$ intercept within 2σ from the $(^{40}Ar/^{36}Ar)_{atm}$ value. All errors are quoted at the 2σ level uncertainty including the error on the irradiation J factor.

In-situ $^{40}Ar/^{39}Ar$ dating technique was performed using a pulsating laser in the UV domain on 200–300 μm-thick sections. Samples were irradiated with fast neutrons in Pavia (Italy) for 20 h, and analysis was performed at Géosciences Montpellier with an ARGUS VI multi-collection mass spectrometer. The ablation of samples were performed using a Nd:YAg laser at λ ~266 nm, with a spot size of 100 μm pulsing for 2 min. Each analysis gives a bulk age representing the ablated domain, and all analyses from each sample are statistically treated using a Kernel Density Estimation (KDE) realized with the DensityPlotter program (Vermeesch, 2012). The KDE presents the measured ages in Ma (X axis) according to the probability density estimation of ages (Y axis).

3.4. Rb-Sr method

Prior to in situ dating using the Rb-Sr method, the microdomains were selected on the basis of their mineral homogeneity, verified by SEM and EPMA (Supplementary Material 1). In-situ Rb-Sr isotopic analyses were conducted at the GeoRessources laboratory, Nancy, France. An Agilent 8900 ICP-MS/MS instrument, coupled to an ESI 193 nm, ArF excimer laser ablation (LA) system with a two-volume 'TwoVol2' ablation chamber, was used to determine $^{87}Rb/^{86}Sr$ and $^{87}Sr/^{86}Sr$ ratios of on selected portions of thin-sections analyzed by EPMA. Analyses were performed following the procedure described by Rösel and Zack (2022) using reference material of Jegal et al. (2022). The Rb-Sr method was applied to all the samples, with 50 to 60 points (50 μm spot). LA-ICP-MS/MS data were processed using the Iolite 4 software (Paton et al., 2011). An identical integration period of 25 s was chosen for the different sample analyses to ensure an interval of stable ablation signal for the different analyses of minerals. The processed and calibrated data for $^{87}Sr/^{86}Sr$ and $^{87}Rb/^{86}Sr$ ratios were plotted in conventional isochron plots and calculated for Rb-Sr isochron ages and the Sr isotope initial ratios by using IsoplotR (Vermeesch, 2018).

4. Results

4.1. Structural and mineralogical investigations of shear zones

4.1.1. Argentera ECM

The BSZ and ISZ are characterized by a progressive deformation gradient at the scale of several 100's of meters (e.g. Sanchez et al., 2011a). Their strike is oriented approximately N130°E, with a sub-vertical dip (Fig. 2A), and mineral lineations are sub-horizontal (slightly dipping to the SE). Ductile deformation progressively increases from undeformed Variscan gneiss-migmatites with stretched partial melting leucosomes (Fig. 3B) towards ultra-mylonites in the core of shear zones. Muscovite and K-feldspar clasts from the protolith are preserved and show a dextral sense of shear. Shear indicators include asymmetrical

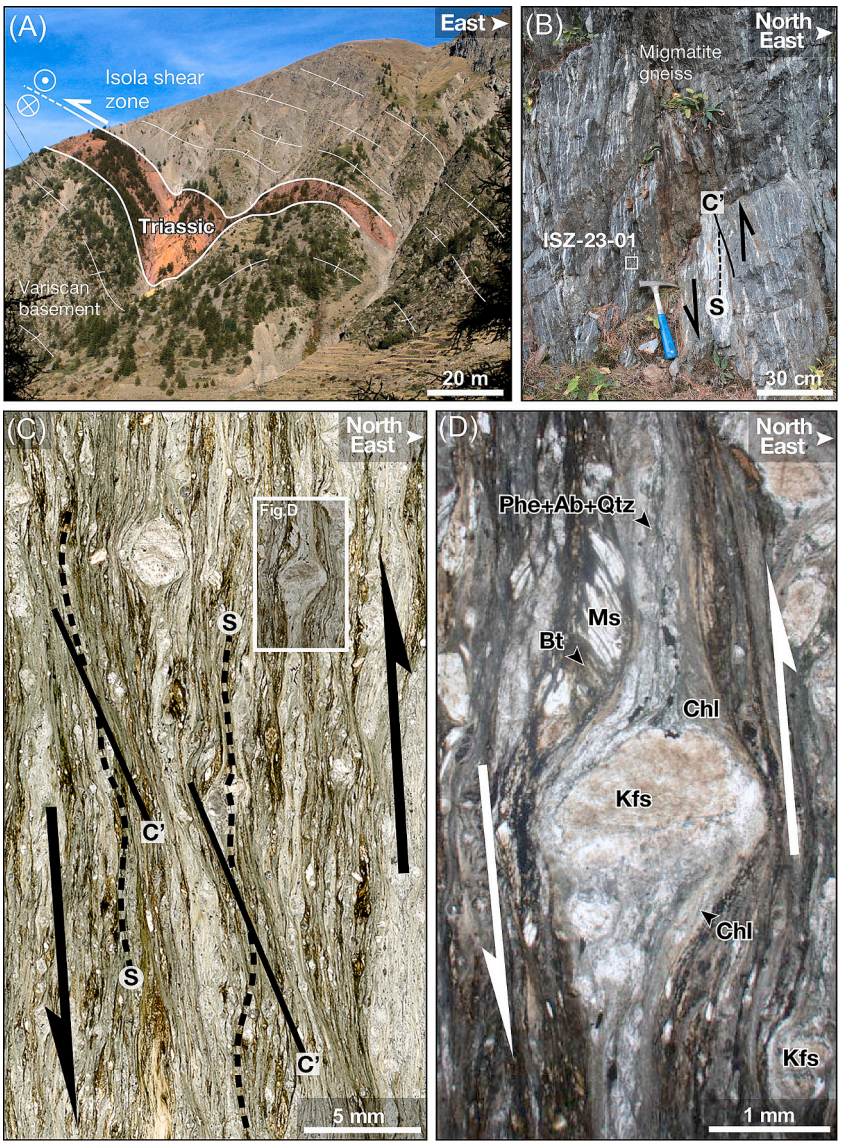

Fig. 3. A) Landscape view of Isola shear zone (ISZ). B) Outcrop view with vertical Alpine foliation and stretched (Variscan) migmatite leucosomes. C) Thin-section view of mylonitic microstructure of sample ISZ-23-01, with asymmetrical pressure-shadows and S-C (C′) criteria indicating a dextral deformation. D) Microscope photography of sample 23-SZI-01. Orthoclase (Kfs), muscovite (Ms), phengite (Ph), albite (Ab), biotite (Bt), chlorite (Chl). See location of sample and pictures in Fig. 2A.

pressure-shadows, C-S and C′ structures (Fig. 3C). In the matrix, minerals are replaced by bands of phengite and chlorite (Fig. 3D). Inhomogeneous phengite-chlorite aggregates, measuring from approximately ~200 μm (sample BSZ-23-03) to ~500 μm (sample BSZ-23-01) are formed in pressure-shadows, intercalated with grains of albite, biotite and Ti-oxides smaller than 20 μm.

4.1.2. Pelvoux ECM

In the Pelvoux ECM, the east-west trending top-to-south shear zone of the Valgaudemar Valley, in the southern part of the massif has been targeted (Figs. 2B, 4A). The mylonite, striking 80–85°E (Fig. 2B) is highly foliated with elongated minerals forming a steeply dipping down-dip lineation, cross-cut by chlorite-rich horizontal veins (Fig. 4B). The shear criteria (asymmetrical pressure shadows, S-C structures) indicate a reverse top-to-the south sense of shear (Fig. 4C). Microstructural analysis of sample V-22-02 thin section (Fig. 4D) reveals K-feldspar porphyroclasts of up to ~1 mm surrounded by long and homogeneous shear bands composed of chlorite, or an assemblage of phengite + albite. These bands are quite large, measuring approximately ~300 μm or more, while individual grains of chlorite or phengite are smaller than 50 μm. The ductile deformation is underlined by shear bands indicating a top-to-south movement (Fig. 4D). Unlike the Argentera ECM, this sample is devoid of any inherited muscovite, presenting only neo-formed white mica (phengite).

4.1.3. Beaufortain ECM

In the Beaufortain ECM, we sampled a top-to-west shear zone north of the Mont Blanc shear zone (Figs. 2C, 5A), within a deformed Carboniferous basin. This shear zone corresponds to an inverted normal fault defining a tilted block (Fig. 2C). Tectonic motion on the shear zone corresponds to a pure reverse deformation, with down-dip mineral lineations (Fig. 5B, C, D). Microstructural analysis of sample BEA-22-01 (Fig. 5C) presents elongated and fragmented orthoclase porphyroclasts smaller than 2 mm, surrounded by an assemblage of chlorite, phengite and albite, which are distributed relatively homogeneously throughout the sample. Phengite appears as aggregates smaller than 20 μm, forming approximately 200 μm wide assemblages with albite. Phengite is also found as inclusions in chlorite bands as needles of variable length

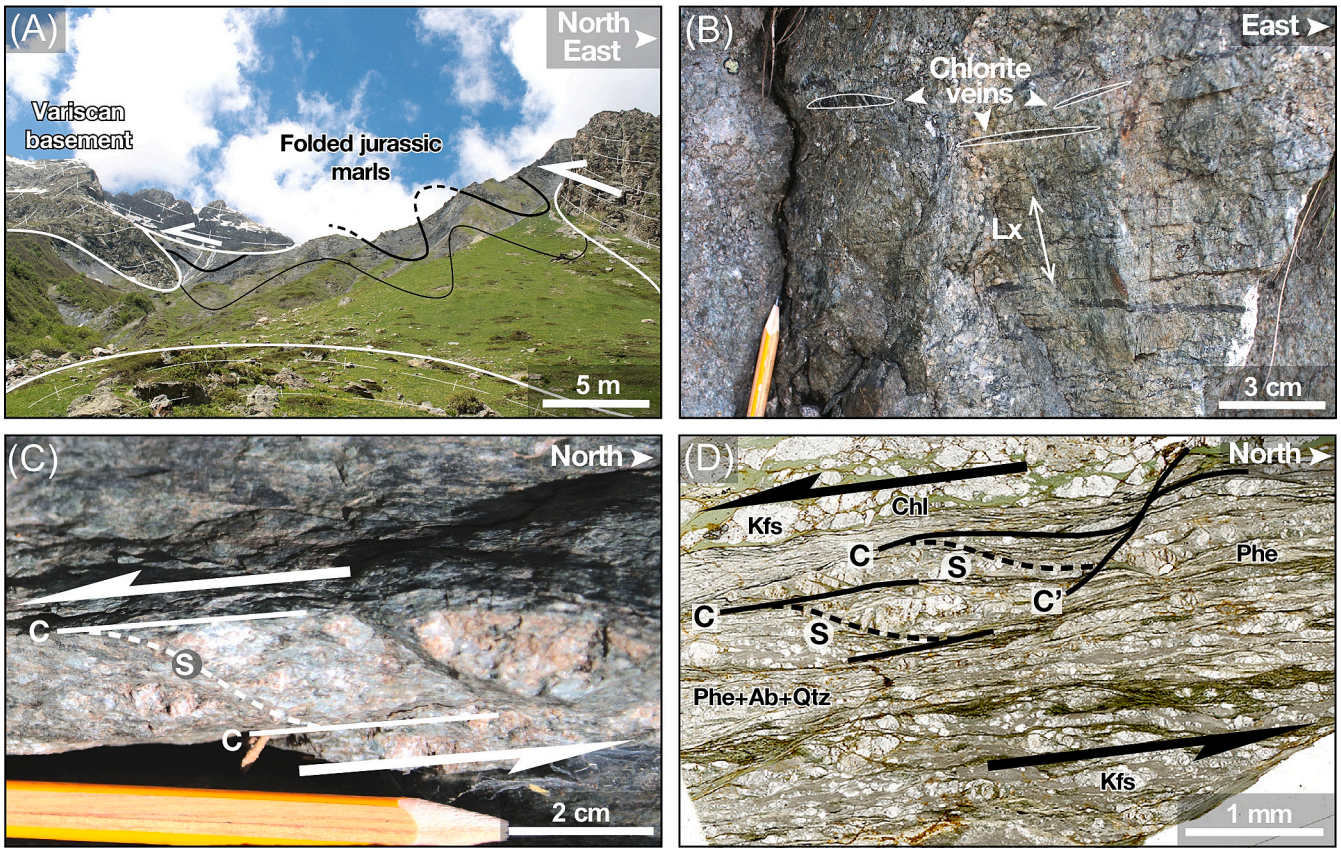

Fig. 4. A) View of the Valgaudemar shear zone thrusting over the Variscan crystalline basement on top of the folded Jurassic marls. B) The shear zone plane with a vertical mineral lineation (Lx) and horizontal chlorite veins. C) Structural C-S relationships indicating a top-to-South sense of shear. D) Thin-section view exhibiting a top-to-south sense of shear, with asymmetrical pressure-shadows and S-C (C′) criteria. Orthoclase (Kfs), phengite (Ph), albite (Ab), chlorite (Chl). See location in Fig. 2B.

ranging between 10 and 50 μm, indicating local equilibrium with chlorite. Identification of elongated K-feldspar grains in the main foliation shows signs of ductile deformation.

4.2. Mineral chemistry and thermobarometry

SEM and EMPA investigation have shown the presence of homogeneous phengite and chlorite domains (Fig. 6; Supplementary materials 2–3). Plots assessing the homogeneity of phengite and chlorite from samples ISZ-23-01, BSZ-23-03, V-22-01, and BEA-22-1 are available in Supplementary Material 2 (Fig. S1 and Fig. S2). For clarity, only the Na vs. Si plot for phengite and the Mg vs. Fe plot for chlorite are shown in Fig. 7A, B and C, as they provide the most relevant insights for the thermobarometry discussion.

4.2.1. Argentera ECM

Argentera shear zone samples exhibit limited variability in phengite composition from 0 to 0.04 apfu in Na content and 3.17 to 3.29 apfu in Si content of both samples ISZ-23-01 and BSZ-23-03 (Fig. 7A). The Mg and Fe contents of chlorite show a homogeneous composition for chlorite at ca. 1.8 apfu Mg and 2.7 apfu Fe for ISZ-23-01 sample. Only one analysis was obtained for sample BSZ-23-01, which is not far from the sample ISZ-23-01 group. This limited chemical variability is interpreted as a single phengite and chlorite population which is similar in the two shear-zones. This interpretation is supported by chemical maps of X_{Mg} and Si (apfu) contents (Fig. 6A). Computations based on the chlorite and phengite compositions constrain the P-T conditions between 275 and 350 °C and ~2 to 4 kbar (Fig. 8A).

4.2.2. Pelvoux ECM

The Valgaudemar shear zone displays variability considering its phengite composition, with Si content varying from 3.17 to 3.29 apfu but little or no variation of the Na content, from 0 to 0.05 apfu (Fig. 7A). The chlorite composition appears also homogeneous with only two points which differ from the main group. Chlorite composition varies from 1.81 to 2.16 for the Mg content and from 2.14 to 2.5 for the Fe content (Fig. 6B). However, these variations remain minor and allow us to consider a single population of phengite and chlorite. The homogeneity is supported by mapping of Si and X_{Mg} contents from phengite and chlorite as composition appears homogeneous at the map scale (Fig. 6B). P-T computations based on chlorites and phengites (Fig. 8B) indicate temperatures of ~225–375 °C and pressures of ~2–5 kbar.

4.2.3. Beaufortain ECM

The Beaufortain shear zone exhibits the most heterogeneous phengite composition. Two groups can be identified in the plot of Na vs. Si content. The first group (Na-rich and Si-poor) exhibits Na content from 0.018 to 0.034 apfu and Si content from 3.14 and 3.29 apfu. The second group (Na-poor and Si-rich) is characterized by a much higher Si content from phengite than any other shear zones, ranging from 3.34 to 3.46 apfu and Na content ranging from 0 to 0.14 apfu (Fig. 7C). However, the Mg and Fe contents of chlorites are homogeneous with very little variations from 2.19 to 2.46 apfu for their Mg content and 2.68 to 2.91 apfu for their Fe content (Fig. 7C). According to Lanari et al. (2012), no distinct generation of chlorite can be identified from the Mg vs. Fe plot. However, two generations of phengite appear to be present, associated with different pressure conditions during their formation. Heterogeneity is evidenced in the chemical mapping of X_{Mg} in chlorite and Si content in phengite. Some areas of the chlorite mapping show a higher

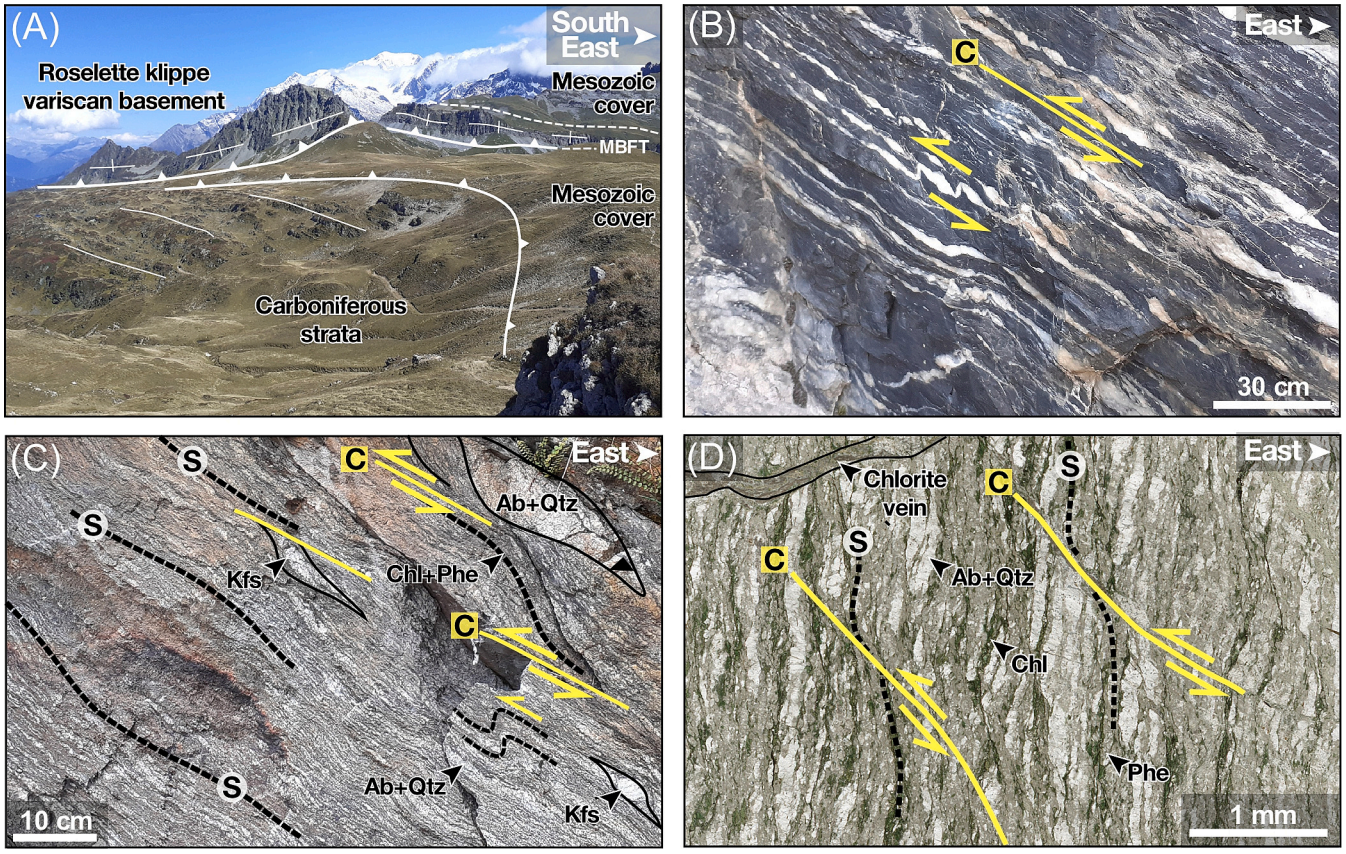

Fig. 5. A) View towards the NE from the Beaufortain massif towards the Roselette klippe. B) top-to-west sense of shear exhibited by asymmetrical folds of calcite veins within Jurassic marbles. C) top-to-west S-C relationships within a mylonitized granite from the Beaufortain crystalline basement. D) vertical cleavage (S) and top-to-west shear planes (C) within the dated carboniferous meta-arkose sample sample (BEA-22-01). See location of sample and pictures in Fig. 2C.

concentration of X_{Mg} than others, but no clear chronological relationship can be established between the two phases. Similarly, one area of the phengite mapping appears depleted in Si, without any obvious chronological correlation. The P-T computations based on chlorites and phengites from XMapTools (Fig. 8C) indicate similar temperatures of ~300 °C for the two phengite generations but show decrease in pressures from ~4 to ~2 kbar for groups 1 and 2, respectively.

4.3. $^{40}Ar/^{39}Ar$ geochronology

4.3.1. Argentera ECM

The results of $^{40}Ar/^{39}Ar$ step-heating experiments for three samples collected on the two parallel shear zones (the Isola and Bersezio shear zones), which are part of the same right-lateral system, are shown on Fig. 9 (and Supplementary Material 4). Sample SZI-23-01 from the ISZ (Fig. 9A) presents a U-shape age spectrum that is representative of Ar excess in LT and HT steps. This sample gives a mean age of 42.3 ± 4.1 Ma corresponding to the central part of the spectrum and to ~70 % of the released ^{39}Ar. We retained a maximum age of 34.5 ± 1.5 Ma, related to the excess Ar in this sample and corresponding to the mean age of two aligned steps with minimum apparent age. Sample BSZ-23-01 from the Bersezio shear zone (Fig. 9B) shows a staircase shape in the LT part of the spectrum, indicative of Ar loss. We retained a mean age of 34.7 ± 1.3 Ma for the flat part of the spectrum corresponding to ~80 % ^{39}Ar released. Sample BSZ-23-03 from the Bersezio shear zone also shows a U-shape age spectrum, indicative of slight excess argon in LT and HT steps. However, this sample yields a plateau age in the central part of the spectrum of 26.2 ± 0.3 Ma, corresponding to 64.9 % of released ^{39}Ar (Fig. 9C).

In-situ $^{40}Ar/^{39}Ar$ dating has also been performed on the same samples and these results are shown on Fig. 9 (and Supplementary Material 5). The three samples dated by this method in the shear zones of the Argentera massif give consistent results. Sample BSZ-23-01 is the only sample, with a density of 11 analysis, yielding an almost unimodal distribution (in orange) corresponding to an age of 30.7 ± 0.2 Ma (Fig. 9A). Two analyses yield ages that do not appear to agree with this main age and may correspond to a less constrained age of around ~42 Ma. Sample BSZ-23-03 shows a three-fold age density plot distribution (Fig. 9B), with age peaks at 27.9 ± 0.2 (5 analyses), 41.6 ± 0.5 (14 analyses) and 70.8 ± 1.0 Ma (8 analyses). Three individual analyses yield ages older than 80 Ma. Sample ISZ-23-01 (Fig. 9C) shows a rather similar age density distribution to the sample BSZ-23-03, with a younger peak at 31.6 ± 0.5 Ma (9 analysis), a second age peak at 44.6 ± 0.7 Ma (6 analyses), a third older one at 72.2 ± 1.1 Ma (4 analyses) and one individual analysis corresponds to an age of ~110 Ma.

4.3.2. Pelvoux ECM

Only the step heating $^{40}Ar/^{39}Ar$ technique was carried out on sample V-22-02. It shows a complex pattern highlighted by a U-shaped spectrum with a staircase shape in its central part with increasing apparent ages between 50 and ~80 Ma, representing 76 % of ^{39}Ar released (Fig. 9D). Therefore, it is impossible to determine a meaningful or robust age for this sample and its complex interpretation is discussed further in Section 5.2.

4.3.3. Beaufortain ECM

Only the step heating $^{40}Ar/^{39}Ar$ technique was performed on sample BEA-22-02 (Fig. 9E). As for the sample V-22-02, this experiment also shows a U-shape spectrum which seems to affect mainly the first and last two steps. In addition, the central part shows a complex and irregular

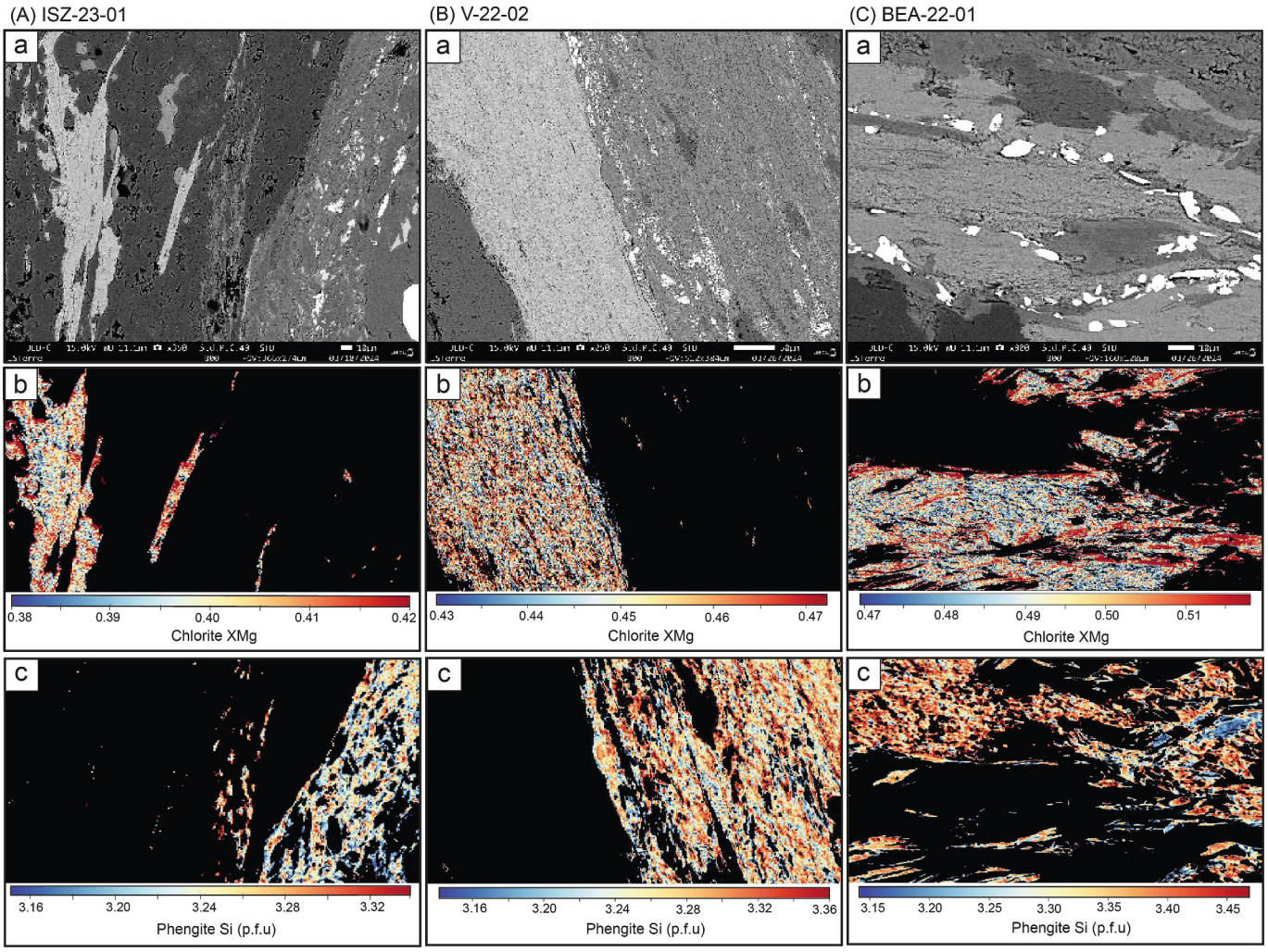

Fig. 6. Representative chemical-microstructure relationships of investigated Alpine shear zones from Mercantour Massif (A, sample ISZ-23-01; B, sample V-22-02) and Beaufortain Massif (sample BEA-22-01). Grayscale top photographs are SEM back-scatter images and middle and lower pictures are compositional maps computed from EPMA analysis. Chlorite XMg (Mg/Mg + Fe) and Phengite Si (pfu) contents are homogenous at the scale considered for dating, except for the Beaufortain sample (C), which shows some slight core rim variations from high Si cores (Group 1) towards low Si rims (Group 2), see Fig. 7.

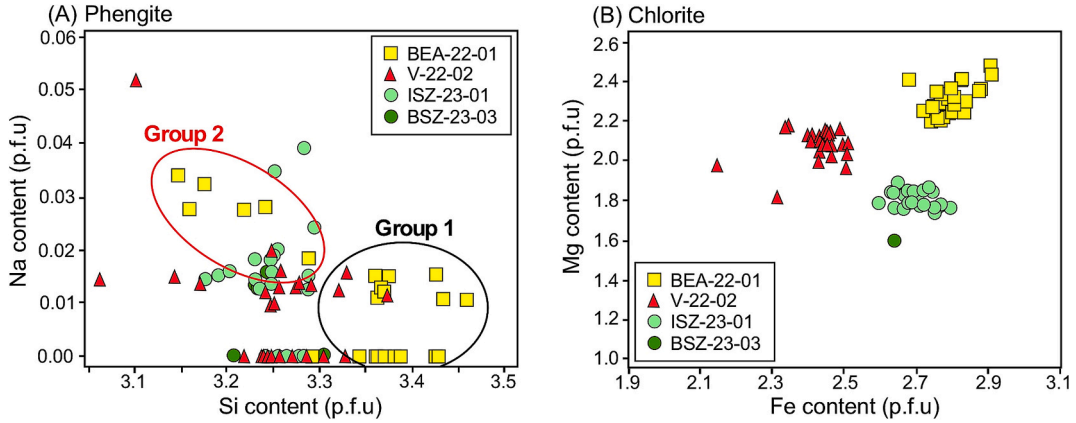

Fig. 7. Mineral composition of investigated shear zone chlorites and phengites. A) Na vs. Si content of Phengites. B) Mg vs. Fe content of chlorites. The homogeneity of mineral chemical variations observed in all samples does not allow to discretize different mineral generation with respect of their microstructural position, except in sample BEA-22-01 from Beaufortain Massif, where two phengite groups are highlighted (Group 1, core compositions and Group 2, rim compositions, cf. Fig. 6).

staircased shape with apparent ages increasing from ~15.4 to ~25 Ma (Fig. 9E). Further, the central part can be divided into two parts: LT steps (representing ~45 % of released ^{39}Ar) giving a slight staircase shape with increasing ages from 15.4 ± 0.4 to 18.5 ± 0.2 Ma, and the HT steps presenting some age variations around ~30 Ma (representing 48 % of released ^{39}Ar).

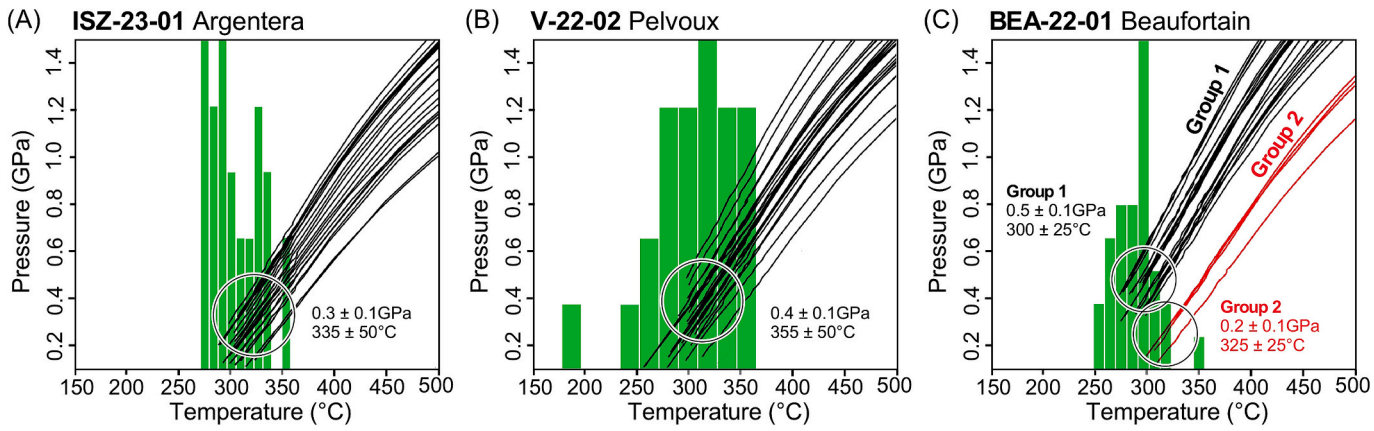

Fig. 8. PT estimates based on chlorite-phengite thermobarometry. Sample ISZ-23-01 mylonite is from the Argentera Massif; sample V-22-02 mylonite is from the Pelvoux Massif; sample BEA-22-01 is from the Beaufortain Massif. Note the homogeneity of the temperatures obtained, around 355 °C, except for the Beaufortain sample, which shows two groups, highlighted by a decrease in pressure from the core (Group 1) to the rim (Group 2) of the analyzed phengites.

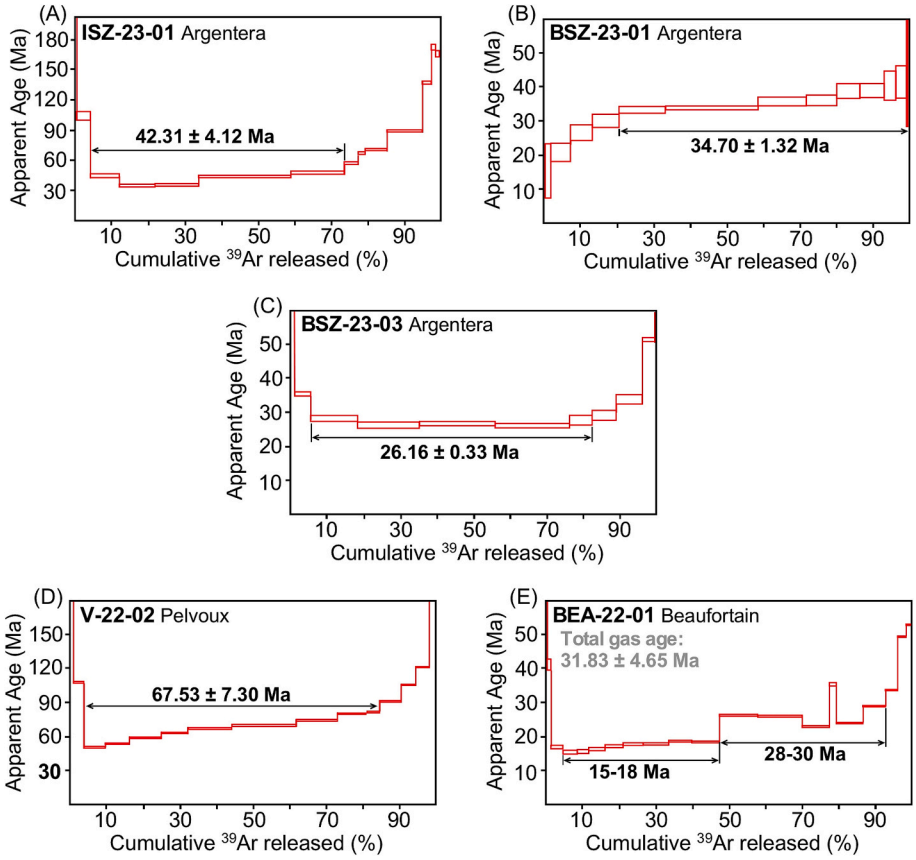

Fig. 9. $^{40}Ar/^{39}Ar$ step heating results of Alpine External Crystalline Massif shear zones. A, mylonite sample ISZ-23-01 from the Argentera massif. B, mylonite sample BSZ-23-01 from the Argentera massif. C, mylonite sample BSZ-23-03 from the Argentera massif. D, mylonite sample V-22-02 from the Pelvoux massif. E, mylonite sample BEA-22-01 from the Beaufortain massif.

4.4. Rb-Sr geochronology

4.4.1. Argentera ECM

Rb-Sr ages obtained in the Argentera massif are slightly younger than, or similar to, the $^{40}Ar/^{39}Ar$ ages (Supplementary Material 6). Sample ISZ-23-01 isochron gives an age of 24.9 ± 6.1 Ma, which is in agreement with the $^{40}Ar/^{39}Ar$ dating performed on this sample, within uncertainties (Fig. 11A). Sample BSZ-23-01 appears to have 2 distinct isochrones, one indicating an old age of 177 ± 36 Ma (Fig. 11B) and the other one indicating a younger age of 38 ± 22 Ma (Fig. 11C). This related uncertainty to the Rb-Sr age is quite high due to the narrow spread of the Rb/Sr ratios. This homogeneity is in agreement with the chemistry of phengite described in the previous section. Sample BSZ-23-03 has an isochron age of 21.8 ± 1.4 Ma (Fig. 11D). Points 1, 2, 3, 4, 5 on the isochron correspond to the biotite that crystallized in pressure-shadow domains of sample BSZ-23-03. It appears that biotite contains higher Rb concentrations than phengite minerals, which may explain the higher spread of Rb/Sr ratios and hence returns an age with a lower uncertainty.

4.4.2. Pelvoux ECM

Rb-Sr dating of sample V-22-02 shows a well-defined isochron correlation yielding an age of 79.7 ± 3.7 Ma (MSWD = 1.1) (Fig. 11E).

4.4.3. Beaufortain ECM

The Rb-Sr dating of sample BEA-22-02 yielded an isochron with an age of 30.7 ± 4.1 Ma (Fig. 11F). Most of the Rb-Sr analyses are homogeneously distributed, and thus the isochron is mainly driven by the points 33, 39, 13 (Fig. 11F), which probably represent a distinct phengite population as their Rb/Sr ratio is higher.

5. Discussion

5.1. Insights for the significance of Rb-Sr and $^{40}Ar/^{39}Ar$ dating methods in shear zones

The interpretation of shear zone dates obtained by $^{40}Ar/^{39}Ar$ and Rb/Sr methods in relation to cooling, fluid circulation or to deformation-induced (re)crystallization remains controversial. Many authors have shown that fluids play a significant role in the resetting of both systems (e.g., Montemagni and Villa, 2025; Tartese et al., 2011 and references therein). Besides, recrystallization appears a major process for resetting of both systems and may act in presence or relative absence of fluids (e.g., Kellett et al., 2016, 2024). Some authors also documented a decoupling of these methods with shear zone $^{40}Ar/^{39}Ar$ ages being older than Rb-Sr ages along some Alpine transects (e.g., Challandes et al., 2008) and elsewhere (Kellett et al., 2024). These authors suggested that the Rb-Sr method is more prone to resetting in case of post-crystallization fluid circulation. Results obtained in the three studied massifs along the SW Alps provide insights into the understanding of Rb-Sr and K-Ar systems in shear zones. Our dataset shows, as in previous studies (e.g., Kellett et al., 2016, 2024) that relatively flat step-heat $^{40}Ar/^{39}Ar$ spectra for some shear zones are inconsistent with the dispersion observed in in-situ $^{40}Ar/^{39}Ar$ and Rb-Sr dates from the same samples. To summarize, several cases are highlighted in the present study:

- In the Argentera massif, the Rb-Sr ages are systematically younger than in-situ $^{40}Ar/^{39}Ar$ ages in the same sample. This is probably related to the concentration in Rb and Sr being significantly higher in the metasomatic rims of phengite than in the inherited cores. In this case, the formation of localized shear bands, at a relatively low temperature (275 °C) allowed the previous minerals to remain globally unaltered. This effect could be related to the specificity of the dating methods: while the $^{40}Ar/^{39}Ar$ method allows to consider each mineral generation based on its volumetric fraction, the Rb-Sr method will emphasize the generation with the more significant spread in Rb-Sr composition, resulting in an isochron correlation. The Rb-Sr system appears to be more sensitive to hydrothermal reset, as these elements are mobile in fluids (Kellett et al., 2024) and also more easily re-incorporated in the minerals than Ar, due to their radius and charge. Finally, the Rb-Sr system appears to be more robust than the K/Ar system with respect to the thermal and deformation induced resetting, also because Ar is more mobile and can be more easily lost during such events.
- In the Pelvoux massif, the ~80 Ma Rb-Sr age appears unaffected by later Alpine activity while the K/Ar system has been partially reset. The obtained $^{40}Ar/^{39}Ar$ age has no geological significance due to incomplete recrystallization (and thus reset of the K/Ar system) of the sample, or because of mixing of population ages. This case highlights an example where the second tectonic event is of lower temperature than the previous phengite crystallization in the shear zone. Further, the shear zone was not reactivated at 35–30 Ma, and still bears a lineation compatible with the first tectonic phase. It follows, in this case, that phengite was not recrystallized and there was no significant fluid circulation, due to the high obliquity of the shear zone. In this case, a partial Ar loss occurred due to a temperature close to 350 °C, but the Rb-Sr system was kept intact.

5.2. Deformation conditions and timing in the ECMs

5.2.1. Pelvoux massif

In the Pelvoux massif, mainly Oligocene (35–27 Ma) ages were documented in basement shear zones, located in the northern and eastern parts of the massif (Bellanger et al., 2015; Simon-Labric et al., 2009). These ages are related to the sedimentary burial under the flysch which developed by lithosphere flexuring in front of the PFT (e.g., Seward et al., 1999), followed by underthrusting beneath the PFT between 34 and 30 Ma (Bellanger et al., 2015; Simon-Labric et al., 2009). However, the shear zones in the SW part of the massif had still not been formerly investigated with a geochronological perspective. The Rb-Sr age of 79.7 ± 3.7 Ma obtained in this study, based on homogeneous phengite analysis in sample V-22-02, provides a solid age constraint for the activity of the Valgaudemar shear zone. This chronological constraint confirms that the Pelvoux Massif has undergone a complex and multi-phase tectonic history, including a shear zone activity during the Late Cretaceous. This multiphase history has been evoked in several works (Boschetti et al., 2025a; Tricart, 2004) and is partly due to the Pyrenean-Provence compressional phase. However, due repeated Late Cretaceous to Eocene compressional events (Balansa et al., 2022; Bilau et al., 2023b) and reactivation of E-W structures during the Oligocene underthrusting of the Pelvoux massif (Simon-Labric et al., 2009), this earlier tectonic phase remains poorly described and geochronologically unconstrained. However, a large-scale effect of the Pyrenean-Provence compressional phase has been suggested in the Provence region and the Dévoluy massif, where a large-scale unconformity has been observed (e.g., Balansa et al., 2022). The work of Tricart (2004) establishes some links between this early Pyreneo-Provence compressive phase and a post-Turonian folding phase observed to the south of the Pelvoux massif and in the neighbouring Dévoluy massif. In the Dévoluy, Senonian deposits (~90–72 Ma) rest uncomformably on a folded sedimentary sequence of Lower Jurassic to Aptian-Albian sediments. This sedimentary unconformity is suggestive of erosion occurring before the Senonian, and resulting in a flat unconformity cutting through the folds and thrusts. Combining the geological features of the Dévoluy and the Rb-Sr geochronology of the Valgaudemar shear zone, it can be suggested that the Pyrenean-Provence compressional phase begun at around ~80 Ma and resulted in the folding and uplift of the Dévoluy massif. It is also suggested that the massif basement was involved in thick-skin tectonics with respect to the P-T estimates conditions of the Valgaudemar shear zone of ~300 °C and ~4 kbar with a burial at ~12 km depth of an upper crustal domain close to the Triassic-basement boundary. These new P-T and geochronological constraints provide the first direct evidence of a significant north-south shortening and thickening of the Pelvoux massif during the Cretaceous, as already suggested by east-west folds and thrusts, observed in the southern part of the massif (e.g., Dumont et al., 2022; Ford, 1996). Furthermore, geophysical data indicate that the Pelvoux Massif is characterized by a thick crust visible with geophysical imagery (~40 km; Nouibat et al., 2022; Schwartz et al., 2024), which is not observable in the other ECMs of the Alpine arc. It is thus suggested that the southern Pelvoux massif has been buried during the early Pyrenean-Provence compression implying a crustal thickening of >10 km. In this context, the recent published ZFT data (Boschetti et al., 2025a), indicate that the Valgaudemar shear zone has accommodated part of the Pelvoux exhumation around ~80 Ma, as evidenced by thermal history of the massif (Boschetti et al., 2025a). In addition, it seems from the mineralogical data that little fluid flow occurred during the 30 Ma deformation event, which explains why the Rb-Sr system was kept intact. Unfortunately, the disturbance of the K-Ar system resulted in a complex U-shape step-heating degassing $^{40}Ar/^{39}Ar$ spectrum that is very difficult to interpret in terms of geological or deformation event. This disturbance may result from a reorganization of the Ar signal at grain

scale with progressive and partial reset of the K-Ar system related to the thermal history of the massif.

5.2.2. Deformation conditions and timing in the Argentera massif

The P-T conditions obtained in the Argentera shear zones range between ~275–350 °C and ~2–4 kbar. These estimates are slightly lower than those obtained by Sanchez et al. (2011a). It has been recently showed that the phase diagram approach used in Sanchez et al. (2011a) is less reliable at low grade conditions due to limitations in the thermodynamic databases (Petroccia et al., 2025) compared to the multi-equilibrium approach used here. The obtained *P* values correspond to a burial depth of ~10–12 km during the massif underthrusting below the PFT, with a temperature slightly above the partial retention zone of ZFT resetting (Bigot-Cormier et al., 2006).

Previous step-heating $^{40}Ar/^{39}Ar$ dating yields either young ages (<34 Ma) associated with the Alpine phase, or a mixture of Alpine and inherited Variscan ages, as suggested by KDE < 80 Ma ages (Fig. 10) (e.g., this study; Corsini et al., 2004; Sanchez et al., 2011a, 2011b; Simonetti et al., 2018). Indeed, muscovite porphyroclasts from the BSZ and ISZ preserve Variscan ages of ~340–320 Ma, whereas *syn*-kinematic phengites give clustered Alpine ages of 34, 26, 22 and 20 Ma (Sanchez et al., 2011a). These Alpine ages are related to transpressive, mainly dextral, shear zone activity during the burial of the massif beneath the PFT at 34 Ma, and its subsequent north-south compressional

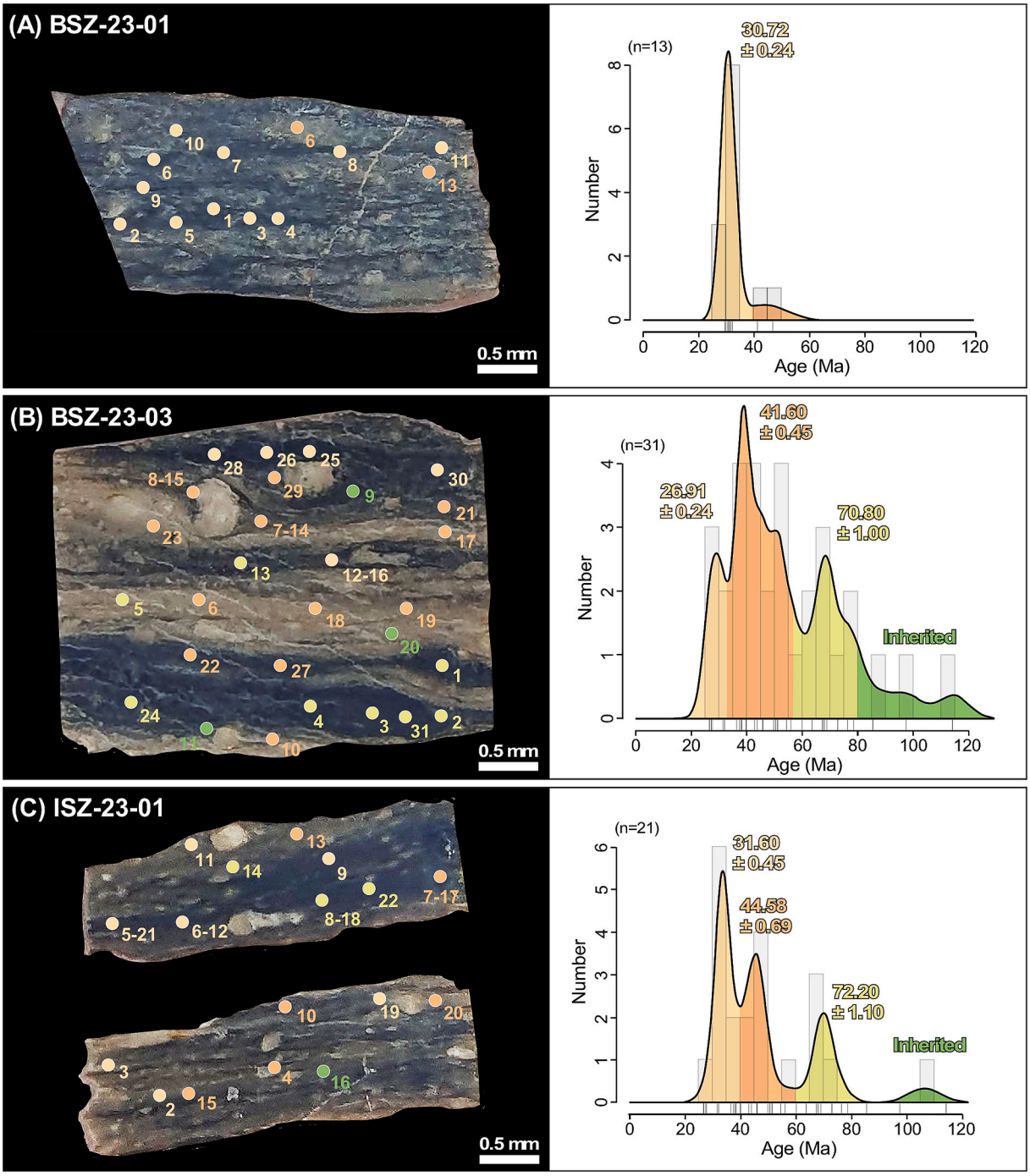

Fig. 10. $^{40}Ar/^{39}Ar$ in situ dating results from the Argentera Massif shear zones. A) sample ISZ-23-01 mylonite. B) Sample BSZ-23-01 mylonite. C) Sample BSZ-23-03 mylonite.

reactivations between 26 and 20 Ma (Sanchez et al., 2011a). In this study, we obtained $^{40}Ar/^{39}Ar$ ages by the step-heating technique: an age of 26.2 ± 0.3 Ma for sample BSZ-23-03, of 34.7 ± 1.3 Ma for sample BSZ-23-01 and only a maximum age at 34.51 ± 1.46 Ma for sample 23-SZI-01. These results are in accordance with those of Sanchez et al. (2011a) and confirm the interpretation of several deformation pulses during and after collisional evolution and subsequent underthrusting below the PFT. The timing of PFT activity, spanning from 34.5 to 29 Ma at the scale of the Western Alps, has been well documented on the basis of $^{40}Ar/^{39}Ar$ dating (Bellanger et al., 2015; Sanchez et al., 2011a; Simon-Labric et al., 2009), U-Pb dating of allanite (Cenki-Tok et al., 2014) and paleontological dating of the flysch sediment (Ceriani et al., 2001).

In-situ $^{40}Ar/^{39}Ar$ laser dating of three samples from the BSZ and ISZ, both from the Argentera massif, yielded three age groups at 28–32 Ma, 42–45 Ma and 71–72 Ma, as well as a wide range of older individual ages that we interpret as more or less reset Variscan ages. The recurrence of these three age peaks suggests a geological significance for these clusters. The youngest population of ages is similar to the $^{40}Ar/^{39}Ar$ ages obtained with the step heating technique and may represent the age of the last main deformation phase. However, the ~42–45 and ~71–72 Ma age peaks represent a new finding in the Argentera shear zones. Late Cretaceous ages (~84–70 Ma) have previously been reported by ZFT dating (Bigot-Cormier et al., 2006) in the NW part of the massif bounded by the Valetta shear zone (St-Etienne de Tinée block) (Fig. 2). These ages are interpreted as an early exhumation of this block like for the Pelvoux massif (Bigot-Cormier et al., 2006; Boschetti et al., 2025a). However, the 42–45 Ma age population is in good agreement with geological evidence of north-south compression during the main (Eocene) Pyrenean-Provence in the south-Alpine foreland (Jourdon et al., 2014).

The Rb-Sr dating of the Argentera massif shear zones yielded three different ages: 35 ± 13 Ma (BSZ-23-01), 24.9 ± 6.1 Ma (ISZ-23-01) and 21.8 ± 1.4 Ma (BSZ-23-03). The large uncertainties in the 35 and 25 Ma age populations is problematic and may represent the same deformation event. It is noticeable that Rb-Sr dates are slightly younger than the $^{40}Ar/^{39}Ar$ dates obtained in the same samples, except for the sample BSZ-23-01 from the Valetta-Bersezio shear zone. However, they coincide with step-heating $^{40}Ar/^{39}Ar$ dates that were obtained along the same shear zone by Sanchez et al. (2011a). The occurrence of slightly younger Rb-Sr ages compared to the $^{40}Ar/^{39}Ar$ ages in the same samples, is interesting and suggests that the K-Ar system has retained the deformation age, while the Rb-Sr system has been more sensitive to a late hydrothermal phase in the shear zones (as suggested by Challandes et al., 2008). Indeed, the Argentera massif shows a significant hydrothermal imprint, emphasized by widespread low-temperature recrystallization in the shear zones and highlighted by numerous active hydrothermal sources (e.g., Sanchez et al., 2010). Widespread hydrothermalism may have occurred for several Myr after the main shearing events and may have resulted in Rb enrichments in the phengite rims (still unresolved due to the size of the minerals), thus significantly affecting the isochron correlations. In contrast, this alteration may have had a least significant effect on the $^{40}Ar/^{39}Ar$ ages due to the relative volume fraction of preserved mineral cores.

We propose that the in-situ $^{40}Ar/^{39}Ar$ ages may correspond to several deformation phases, which reactivated the inherited Variscan shear zones, such as Bersezio and Isola ones (Fig. 2). It is proposed that an early deformation phase occurred around ~71 Ma and was only locally preserved in the massif (e.g St-Etienne de Tinée NW block) or within the Valetta-Bersezio and Isola shear zones. This phase was followed by a second one during the underthrusting of the Argentera massif beneath the PFT at ~34–30 Ma, and by late reactivations between ~26 and ~20 Ma (this study; Sanchez et al., 2011a). These late reactivations of shear zones occurred in a reverse, top-to-south context, due to a late transpressive regime affecting the Western Alps (Rolland et al., 2022; Tricart, 2004). The younger Rb-Sr ages, compared to $^{40}Ar/^{39}Ar$ ages from the same samples, may mainly correspond to hydrothermal pulses. It is suggested that hydrothermalism was associated with the crustal scale shear zones strike-slip activity during this period evidenced by Sanchez et al. (2011a). Detectable ductile tectonic reactivation and combined hydrothermalism ended around ~20 Ma in the studied shear zones. This age is similar to the ZFT age obtained in the NE Argentera (Bigot-Cormier et al., 2006), which could correspond to the exhumation of investigated shear zones below 300 °C. Therefore, the studied shear zones probably continued to be active in more brittle conditions, without any further phengite recrystallization (Sanchez et al., 2011b).

5.2.3. *Deformation conditions and timing in the Beaufortain massif*

Two-phase crystallization of phengite is suggested by its composition, as two groups are identified mainly based on their Si content, and indicate two pressure ranges. Even if petrological investigation does not allow a clear core-rim discrimination, it appears that Group 1 phengites correspond to a higher pressure between ~3–5 kbar, while Group 2 phengites correspond to a pressure of ~2 kbar at relatively similar temperature of ~275 °C (Fig. 8). This evolution is in agreement with a two-phase underthrusting and exhumation of the Beaufortain massif located in front of the Mont-Blanc massif.

The step-heating $^{40}Ar/^{39}Ar$ spectra obtained in the Beaufortain sample BEA-22-01 is complex and displays two distinct parts. The low temperature steps of the central part of the spectra show individual steps with apparent ages between ~15 and 18 Ma, while the high temperature steps yields apparent ages around ~30 Ma. The age of the HT steps is compatible with the Rb/Sr isochrone age of 31 ± 4.1 Ma that we obtained on the same sample.

A similar bimodal age distribution with population at ~18–15 Ma another at ~30 Ma was obtained with in situ $^{40}Ar/^{39}Ar$ analyses by Mercier (2023) in the frontal Mont Blanc shear zone, to the north of the study area. The KDE age distribution from Mercier (2023) shows two distinct age peaks, one at 16.3 ± 3.0 Ma (14 analyses) and another at 29.3 ± 1.5 Ma (7 analyses). The 29.3 Ma age is interpreted by Mercier (2023) as an inherited age component, suggesting initiation of the deformation around ~30 Ma during PFT activity. This interpretation is also supported by a 29 Ma U-Pb ages obtained on allanite by Cenki-Tok et al. (2014) and other $^{40}Ar/^{39}Ar$ ages of biotite-phengite (Rolland et al., 2008) in the Mont Blanc massif. The younger age component of ~18–15 Ma has also been extensively documented in the neighbouring Mont Blanc Massif by laser and step-heating $^{40}Ar/^{39}Ar$ technics (Egli and Mancktelow, 2013; Mercier, 2023; Rolland et al., 2008). These ages were interpreted by these authors as reflecting the age of vertical extrusion of the Mont Blanc massif by combined top-to-the east and west transpressive thrusts.

In summary, we propose that the two deformation phases identified in the Beaufortain sample reflect: (1) a first phase of underthrusting recorded in the core of phengites at ~4 kbar and ~ 30 Ma, followed by (2) a second phase of exhumation due to transpressional tectonics at ~2 kbar and 18–15 Ma.

5.3. *Tectonic evolution of the ECMs: superimposed Pyrenean and Alpine phases*

This study shows that the main shear zones active during Alpine orogeny are inherited structures from earlier Variscan anisotropies rather than newly nucleated and that they were reactivated during each tectonic phase. The studied shear zones belong to the southern branch of the 'East Variscan Shear Zone network' (Fig. 12), which was active between 340 and 300 Ma (Corsini and Rolland, 2009; Simonetti et al., 2018). The results obtained in the ECMs have improved our understanding of the chronology and deformation regime, as well as the thermal conditions of SW Alps from south to north since the Late Cretaceous (Fig. 11). A first-order result concerns the thermal conditions of ECMs recorded in shear zones, which show that similar temperatures (275–300 °C) were reached during the different tectonic phases since the end of the Cretaceous, despite pressure variations. Indeed, the temperatures of ~300–350 °C reached in the southern part of the

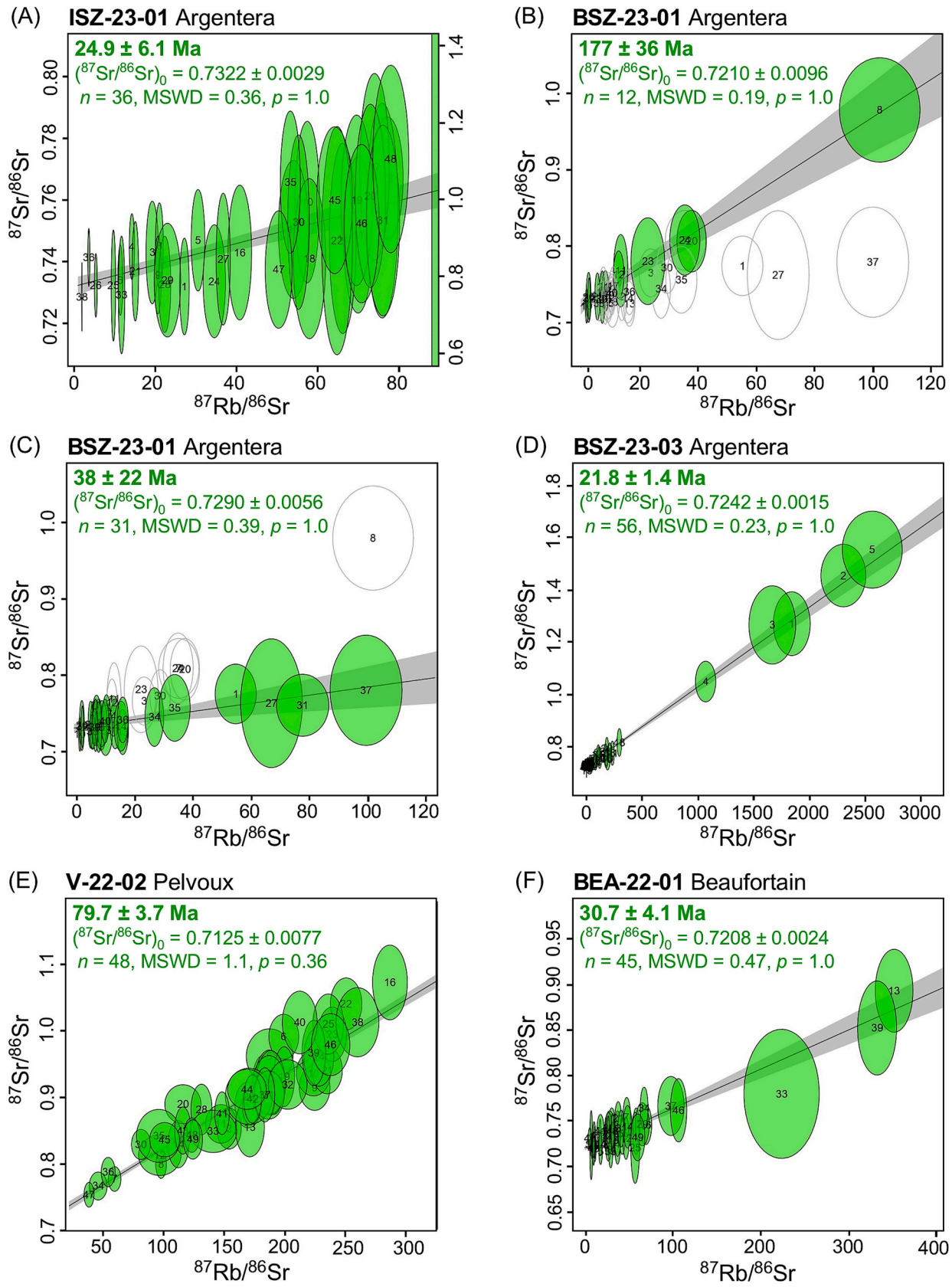

Fig. 11. Rb-Sr in situ dating results of Alpine External Massif shear zones. A) sample 23-SZI-01 mylonite from the Argentera Massif. B) Sample BSZ-23-01 from the Argentera Massif (upper isochrone). C) Sample BSZ-23-01 from the Argentera Massif (lower isochrone). D) Sample BSZ-23-03 from the Argentera Massif. E) Sample V22-02 from the Pelvoux Massif. F) Sample BEA-22-01 from the Beaufortain Massif.

Pelvoux massif during the Late Cretaceous are similar to those reached in the Argentera, Pelvoux and Beaufortain massifs between 34 and 30 Ma.

Based on both the Rb-Sr and K/Ar systems, the shear zones studied across the different ECMs display notable variations in the timing of deformation (Fig. 11). The dates obtained in this study emphasize two, still formerly undocumented in shear zones, early phases of Pyrenean-Provence deformation in the southern part of the Alps, followed by two 'Alpine' phases. In the Argentera and southern Pelvoux massifs, the age signal is clustered around ~80–70 Ma and suggests that a first ductile deformation event occurred at this time. This phase is also supported by ZFT data (Bigot-Cormier et al., 2006; Boschetti et al., 2025a), and documented by other geological evidences, such as the Upper Cretaceous unconformity of the Dévoluy, showing that these massifs were exhumed for a first time around ~80–70 Ma partly controlled by the reactivation of the East Variscan shear zone. This early north-south compression, is documented at the scale of the Provence (Bilau et al., 2023b). A second phase of deformation at ~40 Ma is recorded only in the Argentera massif, and is also well documented by the development of frontal sedimentary basins in this region (Jourdon et al., 2014). This Eocene phase corresponds to the main N-S Pyrenean-Provence compression documented in the literature (e.g., Ford, 1996).

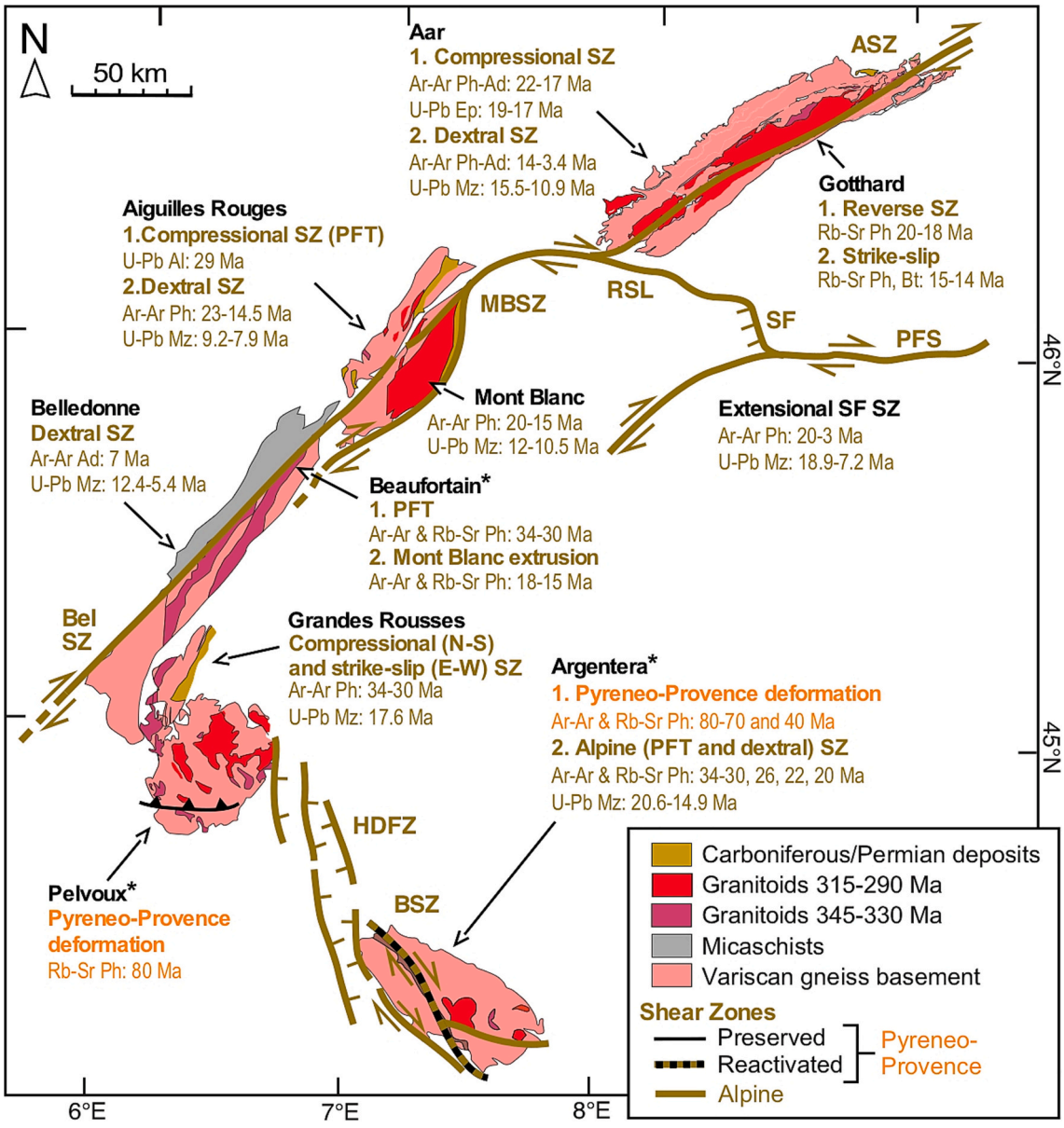

Fig. 12. Compilation of direct ages obtained on low-grade shear zones from the External Crystalline Massifs of Western Alps. Results include Ar-Ar and Rb-Sr on phengite, adularia and biotite and U-Pb on allanite, epidote, garnet and monazite ages. The shear zones reactivate the East Variscan Shear Zone network, initially formed between 340 and 300 Ma. This compilation highlights several stages of reactivation during the Pyreneo-Provence and Alpine compressional phases. *: new data from this paper. ASZ: Aar Shear zone (Ar-Ar on phengite (Ph) from Challandes et al., 2008 and Rolland et al., 2009, U-Pb on epidote (Ep) by Peverelli et al. (2021) and on monazite (Mz) by Ricchi et al. (2019); BelSZ: Belledonne Shear Zone (U-Pb on Monazite and Ar-Ar on adularia by Gasquet et al. (2010) and Janots et al. (2019), BerSZ: Bercesio Shear Zone (Ar-Ar on phengite by Sanchez et al. (2011a), and U-Pb on monazite by Ricchi et al. (2020)), Gottard Massif (U-Pb Grt: U-Pb on garnet ages and Rb-Sr ages from Ceccato et al., 2024). HDFZ: High Durance Fault System (Ar-Ar on phengite by Simon-Labric et al. (2009) and Bellanger et al. (2015), U-Pb on Monazite by Gasquet et al. (2010), MBSZ: Mont Blanc Shear Zone (U-Pb on allanite (Al) by Cenki-Tok et al. (2014) and on Monazite by Bergemann et al. (2019), Ar-Ar on Phengite by Rolland et al. (2008), Egli and Mancktelow (2013) and Mercier (2023); PFS: Periadriadic Fault System, RSL: Rhone Simplon Line and SF: Simplon Fault (Ar-Ar on phengite by Campani et al. (2010); U-Pb on monazite by Gnos et al. (2021)); VSZ: Valetta Shear Zone (Sanchez et al., 2011a).

Further north, these two distinct north-south compressive phases are not yet documented and only 'Alpine' ages (<34 Ma) were obtained. The main deformation event, well documented in shear zones all around the ECMs, corresponds to the phase of European plate underthrusting beneath the PFT, with ages clustered between ~34–30 Ma. This deformation is mostly recorded by the K/Ar system in all massifs whereas the Rb-Sr system is reset, indicating burial of the ECMs to a depth of ~6 km in the Beaufortain and ~ 10 km in the NE Argentera massif. However, the unreset $^{40}Ar/^{39}Ar$ ages in the Argentera massif and the preservation of the ~80 Ma Rb-Sr age in the southern Pelvoux massif indicate that the thermal conditions during underthrusting below the PFT never reached high enough temperatures for a complete reset of the K/Ar and Rb-Sr systems. Furthermore, the preservation of Cretaceous ZFT ages in south Pelvoux (Boschetti et al., 2025a) and NW Argentera (Bigot-Cormier et al., 2006) massifs suggests a peak of temperature below 300 °C during the main phase of PFT underthrusting. We suggest that the Pelvoux ECM significantly thickened in the Late Cretaceous, limiting subsequent underthrusting beneath the PFT at ~34–30 Ma. This rigid behaviour likely explains a reduced burial and less intense metamorphism in the southern part of the Pelvoux massif and western part of the Argentera massif, preserving the P-T conditions and age of the early Pyrenean-Provence deformation phase in shear zones.

The second 'Alpine' deformation corresponds to a transpressive regime, recorded in the Beaufortain massif and in other northern ECMs to the north (Mont Blanc and Aar, Rolland et al., 2022). This phase involved the strike-slip reactivation of vertical crustal shear zones imaged by S-wave tomography (Nouibat et al., 2022; Schwartz et al., 2024), likely driven by the anticlockwise rotation of the Adria plate. In the Argentera massif, this event is recorded between ~26–20 Ma (Bigot-Cormier et al., 2006). Further north, the transpressive regime is highlighted by shear zone activity recorded around ~20–15 Ma in the Beaufortain, Mont Blanc and Aar massifs. This phase coincides with the Mont-Blanc ECM uplift, driven by the re-activation of the Mont-Blanc and Rhône-Simplon shear zones (Campani et al., 2010; Egli and Mancktelow, 2013; Mercier, 2023; Rolland et al., 2008, 2009). In this context, the Beaufortain massif, located in the frontal part of the Mont-Blanc ECM would have recorded two tectonic phases: (i) underthrusting beneath the PFT at 30 Ma and (ii) transpressional deformation and exhumation related to the Mont Blanc pop-up extrusion at 18–15 Ma. After 15 Ma, the Beaufortain and Aiguilles Rouges massifs were exhumed in relation to the propagation of the Alpine deformation front (Bilau et al., 2023a; Boutoux et al., 2016; Girault et al., 2022).

In conclusion, the southern ECMs (Pelvoux and Argentera) shear zones experienced two superimposed deformation phases, associated with the successive Pyrenean-Provence (80–70 Ma) and Alpine (34–30 Ma) tectonics. The first phase resulted in a significant thickening of the European margin, leading to the local erosion of the entire Mesozoic cover and influencing the dynamics of underthrusting during the Alpine phase. As a result, the Pelvoux massif was less buried below the PFT and appears to have been devoid of any tectonic reactivation after 30 Ma. To the north and south of the Pelvoux massif, multiple ductile reactivations occurred at 26, 22 and 20 Ma in the south and 20, 18–15, and <12 Ma in the north. The absence of <20 Ma events in the Argentera ECM is ascribed to its earlier exhumation below equivalent temperatures of 300 °C at 20 Ma, while the Beaufortain and Mont Blanc – Aar ECMs remained at higher temperatures until 10–12 Ma (Rossi and Rolland, 2014).

A major consequence of the superimposition of the two Pyrenean and Alpine thermal phases is that the maximum peak of temperature around 300 °C provided by Raman Spectroscopy of carbonaceous Matter (RSCM) from the ECM sedimentary cover, can correspond to any Pyrenean-Provence or Alpine event, which can lead to significant problems in interpreting the metamorphic record using RSCM data alone (e.g. Bellanger et al., 2015; Célini et al., 2023).

6. Conclusion

The combination of Rb-Sr and $^{40}Ar/^{39}Ar$ ages with P-T estimates allows deciphering the poly-phase deformation in the ECMs of the Western Alps. The approach undertaken in this work shows that it is useful to combine several geochronometers accessible at the 100 μm scale to investigate deformation and hydrothermal phases of low-temperature ductile shear zones. The results highlight a variable behaviour of Rb-Sr and K-Ar systems in shear zones, and show the potential to document previous deformation phases even after multi-stage deformation in a similar temperature range. This study provides new constraints on the timing, conditions and mechanisms of deformation in the southern ECMs of the Western Alps. The inherited crustal-scale Variscan shear zones have been reactivated several times in a thick-skin mode since the Late Cretaceous, highlighting their important role in accommodating deformation over time. From south to north, the three main shear zones studied show a significant difference in the timing of deformation. An early phase of deformation implying the basement around ~80–70 Ma is evidenced in the Argentera and Pelvoux shear zones, but this signal is not documented further north in the Beaufortain and Mont Blanc massifs, where only <34 Ma deformation ages are obtained. The results emphasize four to five phases of deformation that placed the shear zones several times at relatively similar temperature conditions of about 300 °C:

(i) Two Pyrenean-Provence N-S compressional phases at around ~80–70 and ~40 Ma affected the SW Alps. The deformation involved the basement in a thick-skinned mode, with the reactivation of earlier Variscan shear zones in the southwestern Pelvoux and Argentera massifs. The ~80–70 Ma phase is dated by $^{40}Ar/^{39}Ar$ dating on phengite in the Argentera massif, although this geochronological signal is strongly disturbed by further deformation. This signal is better preserved in the south Pelvoux massif, with a Rb-Sr age of 79.7 ± 3.7 Ma. Our results suggest that the south Pelvoux massif reached a temperature around 300 °C at a depth of 10–15 km depth during the Late Cretaceous. This early Pyrenean-Provence phase seems to be the main contributor to the shortening and thickening of this part of the belt. Further north, this early deformation phase is not observed. Afterwards, the Argentera massif shear zones were significantly reactivated during the main Pyrenean-Provence compression at ~40 Ma.

(ii) The ECMs burial below the PFT at 34–30 Ma, and corresponding increase in temperatures is well recorded at the scale of the Western Alps except in the south Pelvoux massif. This lower thermal impact of the PFT in the Pelvoux massif suggests a previous thickening of this part of the Western Alps, which may have acted as a rigid crustal block during PFT activity. During the PFT burial, the Argentera and Beaufortain massifs reached a temperature of 300 °C and a pressure of 2–4 kbar.

(iii) Two deformation pulses at 26 and 22–20 Ma are recorded in the Argentera massif, corresponding to the onset of transpressive deformation induced by the anti-clockwise rotation of Adria, followed by hydrothermalism that completely reset the Rb-Sr system.

(iv) The last phase concerns only the NW Alps and is identified around 18–15 Ma in the Beaufortain massif, which is attributed to transpressional tectonics like in the Mont-Blanc massif. In the Beaufortain ECM, this phase is associated with lower pressures than previous one associated with PFT underthrusting, representing a significant exhumation of Beaufortain massif between 30 and 18 Ma. The increase in pressure conditions up to 3–5 kbar corresponds to a burial of ~12 km.

CRediT authorship contribution statement

L. Boschetti: Writing – review & editing, Writing – original draft,

Visualization, Validation, Investigation, Conceptualization. **C. Boullerne:** Writing – original draft, Investigation, Data curation. **Y. Rolland:** Writing – original draft, Visualization, Validation, Supervision, Investigation, Conceptualization. **S. Schwartz:** Writing – review & editing, Visualization, Validation, Supervision, Investigation, Conceptualization. **G. Milesi:** Writing – review & editing, Methodology, Funding acquisition, Formal analysis, Data curation. **D. Bienveignant:** Investigation. **E. Macret:** Investigation. **D. Charpentier:** Investigation, Funding acquisition. **P. Münch:** Writing – review & editing, Software, Methodology, Formal analysis, Data curation. **J. Mercadier:** Data curation. **A. Iemmolo:** Formal analysis, Data curation. **P. Lanari:** Writing – review & editing, Software, Methodology, Formal analysis, Data curation. **M. Rossi:** Writing – review & editing, Investigation. **F. Mouthereau:** Funding acquisition.

Funding sources

This study was made possible thanks to ministerial funding from the SDU2E doctoral school at University of Toulouse and by additional funding by the RFG-Alps programme, coordinated by the BRGM and the INSU NEEDS project.

Declaration of competing interest

The authors declare that they have no known competing financial interests or personal relationships that could have appeared to influence the work reported in this paper. If there are other authors, they declare that they have no known competing financial interests or personal relationships that could have appeared to influence the work reported in this paper.

Acknowledgements

This work is part of an ongoing collaboration with the BRGM, under the supervision of A. Lafhid. This paper benefited from fruitful discussions with E. Jaillard and C. Basile, and was significantly enhanced following the detailed reviews of A. Ceccato and an anonymous reviewer. We thank W. Bouits for thin section preparation and C. Pfeiffert for his help with the acquisition and processing of Rb-Sr data.

Data availability

The entire dataset is available at in Supplementary material.

References

Agard, P., Handy, M.R., 2021. Ocean subduction dynamics in the Alps. Elements 17 (1), 9–16. https://doi.org/10.2138/gselements.17.1.9.

Balansa, J., Espurt, N., Hippolyte, J., Philip, J., Caritg, S., 2022. Structural evolution of the superimposed Provençal and Subalpine fold-thrust belts (SE France). Earth-science Reviews 227, 103972. https://doi.org/10.1016/j.earscirev.2022.103972.

Bauve, V., Plateaux, R., Rolland, Y., Sanchez, G., Bethoux, N., Delouis, B., Darnault, R., 2014. Long-lasting transcurrent tectonics in SW Alps evidenced by Neogene to present-day stress fields. Tectonophysics 621, 85–100. https://doi.org/10.1016/j.tecto.2014.02.006.

Bellahsen, N., Mouthereau, F., Boutoux, A., Bellanger, M., Lacombe, O., Jolivet, L., Rolland, Y., 2014. Collision kinematics in the western external Alps. Tectonics 33 (6), 1055–1088. https://doi.org/10.1002/2013tc003453.

Bellanger, M., Augier, R., Bellahsen, N., Jolivet, L., Monié, P., Baudin, T., Beyssac, O., 2015. Shortening of the European Dauphinois margin (Oisans Massif, Western Alps): new insights from RSCM maximum temperature estimates and $^{40}Ar/^{39}Ar$ in situ dating. J. Geodyn. 83, 37–64. https://doi.org/10.1016/j.jog.2014.09.00.

Bergemann, C.A., Gnos, E., Whitehouse, M.J., 2019. Insights into the tectonic history of the Western Alps through dating of fissure monazite in the Mont Blanc and Aiguilles Rouges Massifs. Tectonophysics 750, 203–212. https://doi.org/10.1016/j.tecto.2018.11.013.

Bienveignant, D., Nouibat, A., Sue, C., Rolland, Y., Schwartz, S., Bernet, M., et al., 2024. Shaping the crustal structure of the SW-Alpine Foreland: insights from 3D Geological modeling. Tectonophysics 889, 230471. https://doi.org/10.1016/j.tecto.2024.230471.

Bigot-Cormier, F., Sosson, M., Poupeau, G., Stéphan, J.F., Labrin, E., 2006. The denudation history of the Argentera Alpine External Crystalline Massif (Western Alps, France-Italy): an overview from the analysis of fission tracks in apatites and zircons. Geodin. Acta 19 (6), 455–473. https://doi.org/10.3166/ga.19.455-473.

Bilau, A., Bienveignant, D., Rolland, Y., Schwartz, S., Godeau, N., Guihou, A., Deschamps, P., Mangenot, X., Brigaud, B., Boschetti, L., Dumont, T., 2023a. The Tertiary structuration of the Western Subalpine foreland deciphered by calcite-filled faults and veins. Earth Sci. Rev. 236, 104270. https://doi.org/10.1016/j.earscirev.2022.104270.

Bilau, A., Rolland, Y., Dumont, T., Schwartz, S., Godeau, N., Guihou, A., Deschamps, P., 2023b. Early onset of Pyrenean collision (97–90 Ma) evidenced by U–Pb dating on calcite (Provence, SE France). Terra Nova 35 (5), 413–423. https://doi.org/10.1111/ter.12665.

Boschetti, L., Mouthereau, F., Schwartz, S., Rolland, Y., Bernet, M., Balvay, M., et al., 2025a. Thermochronology of the western Alps (Pelvoux massif) reveals the longterm multiphase tectonic history of the European paleomargin. Tectonics 44 (2), e2024TC008498. https://doi.org/10.1029/2024TC008498.

Boschetti, L., Rolland, Y., Mouthereau, F., Schwartz, S., Milesi, G., Munch, P., Bernet, M., Balvay, M., Thiéblemont, D., Bonno, M., Martin, C., Monié, P., 2025b. Thermochronology of the Maures-Tanneron crystalline basement: Insights for SW Europe Triassic to Miocene tectonic history. Swiss Journal of Geoscience. https://doi.org/10.1186/s00015-025-00485-8. In Press.

Boutoux, A., Bellahsen, N., Nanni, U., Pik, R., Verlaguet, A., Rolland, Y., Lacombe, O., 2016. Thermal and structural evolution of the external Western Alps: Insights from (U–Th–Sm)/He thermochronology and RSCM thermometry in the Aiguilles Rouges/Mont Blanc massifs. Tectonophysics 683, 109–123. https://doi.org/10.1016/j.tecto.2016.06.010.

Campani, M., Mancktelow, N., Seward, D., Rolland, Y., Müller, W., Guerra, I., 2010. Geochronological evidence for continuous exhumation through the ductile-brittle transition along a crustal-scale low-angle normal fault: Simplon Fault Zone, central Alps. Tectonics 29 (3). https://doi.org/10.1029/2009TC002582.

Ceccato, A., Behr, W.M., Zappone, A.S., Tavazzani, L., Giuliani, A., 2024. Structural evolution, exhumation rates, and rheology of the European crust during Alpine collision: constraints from the Rotondo granite—Gotthard nappe. Tectonics 43 (6), e2023TC008219.

Célini, N., Mouthereau, F., Lahfid, A., Gout, C., Callot, J.P., 2023. Rift thermal inheritance in the SW Alps (France): insights from RSCM thermometry and 1D thermal numerical modelling. Solid Earth 14 (1), 1–16. https://doi.org/10.5194/se-14-1-2023.

Cenki-Tok, B., Darling, J.R., Rolland, Y., Dhuime, B., Storey, C.D., 2014. Direct dating of mid-crustal shear zones with synkinematic allanite: new in situ U-Th-Pb geochronological approaches applied to the Mont Blanc massif. Terra Nova 26 (1), 29–37. https://doi.org/10.1111/ter.12066.

Ceriani, S., Fügenschuh, B., Schmid, S.M., 2001. Multi-stage thrusting at the "Penninic Front" in the Western Alps between Mont Blanc and Pelvoux massifs. International Journal of Earth Sciences 90 (3), 685–702. https://doi.org/10.1007/s005310000188.

Challandes, N., Marquer, D., Villa, I.M., 2008. PTt Modelling, Fluid Circulation, and $^{39}Ar–^{40}Ar$ and Rb–Sr Mica Ages in the Aar Massif Shear Zones (Swiss Alps). Swiss J. Geosci. 101, 269–288. https://doi.org/10.1111/ter.12066.

Corsini, M., Rolland, Y., 2009. Late evolution of the southern European Variscan belt: exhumation of the lower crust in a context of oblique convergence. C. R. Geosci. 341 (2–3), 214–223. https://doi.org/10.1016/j.crte.2008.12.002.

Corsini, M., Ruffet, G., Caby, R., 2004. Alpine and late-hercynian geochronological constraints in the Argentera Massif (Western Alps). Eclogae Geol. Helv. 97, 3–15. https://doi.org/10.1007/s00015-004-1107-8.

Dall'Asta, N., Hoareau, G., Manatschal, G., Centrella, S., Denèle, Y., Ribes, C., Kalifi, A., 2022. Structural and petrological characteristics of a Jurassic detachment fault from the Mont-Blanc massif (Col du Bonhomme area, France). J. Struct. Geol. 159, 104593. https://doi.org/10.1016/j.jsg.2022.104593.

Di Vincenzo, G., Carosi, R., Palmeri, R., 2004. The relationship between tectono-metamorphic evolution and argon isotope records in white mica: Constraints from in situ 40Ar-39Ar laser analysis of the Variscan Basement of Sardinia. J. Petrol. 45 (5), 1013–1043. https://doi.org/10.1093/petrology/egh002.

Dubacq, B., Vidal, O., De Andrade, V., 2010. Dehydration of dioctahedral aluminous phyllosilicates: thermodynamic modelling and implications for thermobarometric estimates. Contrib. Mineral. Petrol. 159, 159–174. https://doi.org/10.1007/s00410-009-0421-6.

Dumont, T., Schwartz, S., Guillot, S., Malusa, M., Jouvent, M., Monié, P., Verly, A., 2022. Cross-propagation of the western Alpine orogen from early to late deformation stages: evidence from the Internal Zones and implications for restoration. Earth Sci. Rev. 232, 104106. https://doi.org/10.1016/j.earscirev.2022.104106.

Egli, D., Mancktelow, N., 2013. The structural history of the Mont Blanc massif with regard to models for its recent exhumation. Swiss Journal of Geosciences 106, 469–489. https://doi.org/10.1007/s00015-013-0153-5.

Ford, M., 1996. Kinematics and geometry of early Alpine, basement-involved folds, SW Pelvoux Massif, SE France. Eclogae Geologicae Helvetiae 89 (1), 269–295. https://doi.org/10.5169/seals-167902.

Ford, M., Masini, E., Vergés, J., Pik, R., Ternois, S., Léger, J., et al., 2022. Evolution of a low convergence collisional orogen: a review of Pyrenean orogenesis. Bulletin de la Société Géologique de France 193 (1). https://doi.org/10.1051/bsgf/2022018.

Gasquet, D., Bertrand, J.M., Paquette, J.L., Lehmann, J., Ratzov, G., de Ascencao Guedes, R., et al., 2010. Miocene to Messinian deformation and hydrothermal activity in a pre-Alpine basement massif of the French western Alps: new U-Th-Pb and argon ages from the Lauzière massif. Bulletin de la Société Géologique de France 181 (3), 227–241. https://doi.org/10.2113/gssgfbull.181.3.227.

Girault, J., Bellahsen, N., Bernet, M., Pik, R., Loget, N., Lasseur, E., Rosenberg, C., Balvay, M., Sonnet, M., 2022. Exhumation of the Western Alpine collisional wedge:

new thermochronological data. Tectonophysics 822, 229155. https://doi.org/10.1016/j.tecto.2021.229155.
Gnos, E., Mullis, J., Ricchi, E., Bergemann, C.A., Janots, E., Berger, A., 2021. Episodes of fissure formation in the alps: connecting quartz fluid inclusion, fissure monazite age, and fissure orientation data. Swiss J. Geosci. 114, 14. https://doi.org/10.1186/s00015-021-00391-9.
Janots, E., Grand'Homme, A., Bernet, M., Guillaume, D., Gnos, E., Boiron, M.C., et al., 2019. Geochronological and thermometric evidence of unusually hot fluids in an Alpine fissure of Lauzière granite (Belledonne, Western Alps). Solid Earth 10 (1), 211–223. https://doi.org/10.5194/se-10-211-2019.
Jegal, Y., Zimmermann, C., Reisberg, L., Yeghicheyan, D., Cloquet, C., Peiffert, C., et al., 2022. Characterisation of reference materials for in situ Rb-Sr dating by LA-ICP-MS/MS. Geostand. Geoanal. Res. 46 (4), 645–671. https://doi.org/10.1111/ggr.12456.
Jourdon, A., Rolland, Y., Petit, C., Bellahsen, N., 2014. Style of Alpine tectonic deformation in the Castellane fold-and-thrust belt (SW Alps, France): Insights from balanced cross-sections. Tectonophysics 633, 143–155. https://doi.org/10.1016/j.tecto.2014.06.022.
Kellett, D.A., Warren, C., Larson, K.P., Zwingmann, H., van Staal, C.R., Rogers, N., 2016. Influence of deformation and fluids on Ar retention in white mica: dating the Dover Fault, Newfoundland Appalachians. Lithos 254, 1–17. https://doi.org/10.1016/j.lithos.2016.03.003.
Kellett, D.A., Larson, K.P., Skipton, D.R., 2024. Integration of white mica in situ $^{87}Rb/^{87}Sr$ with in situ and step-heat $^{40}Ar/^{39}Ar$ dates in orogenic settings. Lithos 482, 107687. https://doi.org/10.1016/j.lithos.2024.107687.
Koppers, A.A., 2002. ArArCALC—software for 40Ar/39Ar age calculations. Computers Geosci. 28 (5), 605–619. https://doi.org/10.1016/S0098-3004(01)00095-4.
Lanari, P., Guillot, S., Schwartz, S., Vidal, O., Tricart, P., Riel, N., Beyssac, O., 2012. Diachronous evolution of the alpine continental subduction wedge: evidence from P–T estimates in the Briançonnais Zone houillère (France – Western Alps). J. Geodyn. 56-57, 39–54. https://doi.org/10.1016/j.jog.2011.09.006.
Lanari, P., Rolland, Y., Schwartz, S., Vidal, O., Guillot, S., Tricart, P., Dumont, T., 2013. P–T–t estimation of deformation in low-grade quartz-feldspar-bearing rocks using thermodynamic modelling and $^{40}Ar/^{39}Ar$ dating techniques: example of the Plan-de-Phasy shear zone unit (Briançonnais Zone, Western Alps). Terra Nova 26 (2), 130–138. https://doi.org/10.1111/ter.12079.
Lanari, P., Vidal, O., De Andrade, V., Dubacq, B., Lewin, E., Schwartz, S., 2014. XMapTools a Matlab©-based graphic user interface for microprobe X-ray images processing. Comput. Geosci. 62, 227–240. https://doi.org/10.1016/j.cageo.2013.08.010.
Lee, J.Y., Marti, K., Severinghaus, J.P., Kawamura, K., Yoo, H.S., Lee, J.B., Kim, J.S., 2006. A redetermination of the isotopic abundances of atmospheric Ar. Geochim. Cosmochim. Acta 70 (17), 4507–4512. https://doi.org/10.1016/j.gca.2006.06.1563.
Mercier, A., 2023. 4D Reconstruction of Alpine Deformations in the Western Alps. PhD dissertation. Université Claude Bernard Lyon 1. Tel-04390525.
Mohn, G., Manatschal, G., Beltrando, M., Haupert, I., 2014. The role of rift-inherited hyper-extension in Alpine-type orogens. Terra Nova 26 (5), 347–353. https://doi.org/10.1111/ter.12104.
Monié, P., Münch, P., Milesi, G., Bonno, M., Iemmolo, A., 2023. $^{40}Ar/^{39}Ar$ geochronology of crustal deformation. C. R. Geosci. 356 (S2), 1–29. https://doi.org/10.5802/crgeos.209.
Montemagni, C., Villa, I.M., 2025. Dating deformation by the $^{40}Ar/^{39}Ar$ method: a review. Ital. J. Geosci. 144. https://doi.org/10.3301/IJG.2025.06.
Montemagni, C., Zanchetta, S., Rocca, M., Villa, I.M., Morelli, C., Mair, V., Zanchi, A., 2023. Kinematics and time-resolved evolution of the main thrust-sense shear zone in the Eo-Alpine orogenic wedge (the Vinschgau Shear Zone, eastern Alps). Solid Earth 14 (5), 551–570. https://doi.org/10.5194/se-14-551-2023.
Nibourel, L., Berger, A., Egli, D., Heuberger, S., Herwegh, M., 2021. Structural and thermal evolution of the eastern Aar Massif: insights from structural field work and Raman thermometry. Swiss J. Geosci. 114 (1), 9.
Nouibat, A., Stehly, L., Paul, A., Schwartz, S., Bodin, T., Dumont, T., Rolland, Y., Brossier, R., CIFALPS Group, 2022. Lithospheric transdimensional ambient-noise tomography of W-Europe: implications for crustal-scale geometry of the W-Alps. Geophys. J. Int. 229, 862–879. https://doi.org/10.1093/gji/ggab520.
Parizot, O., Missenard, Y., Barbarand, J., Blaise, T., Benedicto, A., Haurine, F., Sarda, P., 2022. How sensitive are intraplate inherited structures? Insight from the Cévennes Fault System (Languedoc, SE France). Geol. Mag. 159 (11−12), 2082–2094. https://doi.org/10.1017/S0016756822000152.
Paton, C., Hellstrom, J., Paul, B., Woodhead, J., Hergt, J., 2011. Iolite: freeware for the visualisation and processing of mass spectrometric data. J. Anal. At. Spectrom 26 (12), 2508–2518. https://doi.org/10.1039/C1JA10172B.
Petroccia, A., Forshaw, J.B., Lanari, P., Iaccarino, S., Montomoli, C., Carosi, R., 2025. Pressure and temperature estimation in greenschist-facies metapelites: an example from the Variscan Belt in Sardinia. J. Metam. Geol. 43 (1), 21–46. https://doi.org/10.1111/jmg.12799.
Peverelli, V., Ewing, T., Rubatto, D., Wille, M., Berger, A., Villa, I.M., Lanari, P., Pettke, T., Herwegh, M., 2021. U–Pb Geochronology of Epidote by Laser Ablation Inductively Coupled Plasma Mass Spectrometry (LA–ICP–MS) as a Tool for Dating Hydrothermal Vein Formation. Geochronology 3, 123–147. https://doi.org/10.5194/gchron-3-123-2021.
Renne, P.R., Deino, A.L., Hames, W.E., Heizler, M.T., Hemming, S.R., Hodges, K.V., et al., 2009. Data reporting norms for $^{40}Ar/^{39}Ar$ geochronology. Quat. Geochronol. 4 (5), 346–352. https://doi.org/10.1016/j.quageo.2009.06.005.
Ribes, C., Ghienne, J.F., Manatschal, G., Dall'Asta, N., Stockli, D.F., Galster, F., et al., 2020. The Grès Singuliers of the Mont Blanc region (France and Switzerland): stratigraphic response to rifting and crustal necking in the Alpine Tethys. International Journal of Earth Sciences 109, 2325–2352. https://doi.org/10.1007/s00531-020-01902-z.
Ricchi, E., Bergemann, C., Gnos, E., Berger, A., Rubatto, D., Whitehouse, M., 2019. Constraining deformation phases in the Aar Massif and the Gotthard Nappe (Switzerland) using Th–Pb crystallization ages of fissure monazite–(Ce). Lithos 342, 223–238. https://doi.org/10.1016/j.lithos.2019.04.014.
Ricchi, E., Gnos, E., Rubatto, D., Whitehouse, M.J., Pettke, T., 2020. Ion microprobe dating of fissure monazite in the western alps: insights from the Argentera Massif and the Piemontais and Briançonnais Zones. Swiss J. Geosci. 113, 15. https://doi.org/10.1186/s00015-020-00365-3.
Rolland, Y., Rossi, M., Cox, S.F., Corsini, M., Mancktelow, N., Pennacchioni, G., et al., 2008. 40Ar/39Ar dating of synkinematic white mica: insights from fluid-rock reaction in low-grade shear zones (Mont Blanc Massif) and constraints on timing of deformation in the NW external Alps. Geol. Soc. Lond. Spec. Publ. 299 (1), 293–315. https://doi.org/10.1144/SP299.18.
Rolland, Y., Cox, S.F., Corsini, M., 2009. Constraining deformation stages in brittle–ductile shear zones from combined field mapping and $^{40}Ar/^{39}Ar$ dating: the structural evolution of the Grimsel Pass area (Aar Massif, Swiss Alps). Journal of Structural Geology 31 (11), 1377–1394. https://doi.org/10.1016/j.jsg.2009.08.003.
Rolland, Y., Bilau, A., Cardinal, T., Nouibat, A., Bienveignant, D., Boschetti, L., et al., 2022. Bridging the gap between long–term orogenic evolution (>10 Ma Scale) and geomorphological processes that shape the Western Alps: insights from combined dating approaches. Geosciences 12 (11), 393. https://doi.org/10.3390/geosciences12110393.
Rösel, D., Zack, T., 2022. LA-ICP-MS/MS single-spot Rb-Sr dating. Geostand. Geoanal. Res. 46 (2), 143–168. https://doi.org/10.1111/ggr.12414.
Rosenberg, C.L., Bellahsen, N., Rabaute, A., Girault, J.B., 2021. Distribution, style, amount of collisional shortening, and their link to Barrovian metamorphism in the European Alps. Earth-Science Reviews 222, 103774. https://doi.org/10.1016/j.earscirev.2021.103774.
Rossi, M., Rolland, Y., 2014. Stable isotope and Ar/Ar evidence of prolonged multiscale fluid flow during exhumation of orogenic crust: example from the Mont Blanc and Aar Massifs (NW Alps). Tectonics 33 (9), 1681–1709.
Sanchez, G., Rolland, Y., Schreiber, D., Giannerini, G., Corsini, M., Lardeaux, J.M., 2010. The active fault system of SW Alps. J. Geodyn. 49 (5), 296–302. https://doi.org/10.1016/j.jog.2009.11.009.
Sanchez, G., Rolland, Y., Schneider, J., Corsini, M., Oliot, E., Goncalves, P., Verati, C., Lardeaux, J., Marquer, D., 2011a. Dating low-temperature deformation by $^{40}Ar/^{39}Ar$ on white mica, insights from the Argentera-Mercantour Massif (SW Alps). Lithos 125 (1–2), 521–536. https://doi.org/10.1016/j.lithos.2011.03.009.
Sanchez, G., Rolland, Y., Jolivet, M., Brichau, S., Corsini, M., Carter, A., 2011b. Exhumation controlled by transcurrent tectonics: the Argentera–Mercantour massif (SW Alps). Terra Nova 23 (2), 116–126. https://doi.org/10.1111/j.1365-3121.2011.00991.x.
Schneider, S., Hammerschmidt, K., Rosenberg, C.L., 2013. Dating the longevity of ductile shear zones: insight from $^{40}Ar/^{39}Ar$ in situ analyses. Earth Planet. Sci. Lett. 369, 43–58. https://doi.org/10.1016/j.epsl.2013.03.002.
Schwartz, S., Gautheron, C., Audin, L., Dumont, T., Nomade, J., Barbarand, J., Pinna-Jamme, R., van der Beek, P., 2017. Foreland exhumation controlled by crustal thickening in the Western Alps. Geology 45, 139–142. https://doi.org/10.1130/G38561.1.
Schwartz, S., Rolland, Y., Nouibat, A., Boschetti, L., Bienveignant, D., Dumont, T., Mouthereau, F., 2024. Role of mantle indentation in collisional deformation evidenced by deep geophysical imaging of Western Alps. Comm. Earth Environ. 5 (1), 17. https://doi.org/10.1038/s43247-023-01180-y.
Seward, D., Ford, M., Burgisser, J., Lickorish, H., WILLIAMS, E.D., MECKEL, L.D., 1999. Preliminary results of fission track analyses in the Southern Pelvoux area, SE France. Mem. Sci. Geol. Padova 51, 25–31.
Simonetti, M., Carosi, R., Montomoli, C., Langone, A., D'Addario, E., Mammoliti, E., 2018. Kinematic and geochronological constraints on shear deformation in the Ferriere-Mollières shear zone (Argentera-Mercantour Massif, Western Alps): implications for the evolution of the Southern European Variscan Belt. Int. J. Earth Sci. 107 (6), 2163–2189. https://doi.org/10.1007/s00531-018-1593-y.
Simon-Labric, T., Rolland, Y., Dumont, T., Heymes, T., Authemayou, C., Corsini, M., Fornari, M., 2009. $^{40}Ar/^{39}Ar$ dating of Penninic Front tectonic displacement (W Alps) during the Lower Oligocene (31–34 Ma). Terra Nova 21 (2), 127–136. https://doi.org/10.1111/j.1365-3121.2009.00865.x.
Sue, C., Tricart, P., Dumont, T., Pêcher, A., 1997. Raccourcissement polyphasé dans le massif du Pelvoux (Alpes occidentales): exemple du chevauchement de socle de Villard-Notre-Dame. Comptes Rendus de l'Académie des Sciences-Series IIA-Earth and Planetary Science 324 (10), 847–854. https://doi.org/10.1016/S1251-8050(97)82520-7.
Tartese, R., Ruffet, G., Poujol, M., Boulvais, P., Ireland, T.R., 2011. Simultaneous resetting of the muscovite K-Ar and monazite U-Pb geochronometers: a story of fluids. Terra Nova 23 (6), 390–398. https://doi.org/10.1111/j.1365-3121.2011.01024.x.
Tricart, P., 2004. From extension to transpression during the final exhumation of the Pelvoux and Argentera massifs, Western Alps. Eclogae Geologicae Helveticae/Eclogae Geologicae Helvetiae 97 (3), 429–439. https://doi.org/10.1007/s00015-004-1138-1.
Vermeesch, P., 2012. On the visualisation of detrital age distributions. Chem. Geol. 312, 190–194. https://doi.org/10.1016/j.chemgeo.2012.04.021.

Vermeesch, P., 2018. IsoplotR: a free and open toolbox for geochronology. Geosci. Front. 9 (5), 1479–1493. https://doi.org/10.1016/j.gsf.2018.04.001.
Vidal, O., Parra, T., Vieillard, P., 2005. Thermodynamic properties of the Tschermak solid solution in Fe-chlorite: application to natural examples and possible role of oxidation. Am. Mineral. 90 (2–3), 347–358.
Warr, L.N., 2021. IMA–CNMNC approved mineral symbols. Mineral. Mag. 85 (3), 291–320.